CrossMark

ORIGINAL PAPER

P–T–t evolution of eclogite/blueschist facies metamorphism in Alanya Massif: time and space relations with HP event in Bitlis Massif, Turkey

Mete Çetinkaplan · Amaury Pourteau · Osman Candan · O. Ersin Koralay · Roland Oberhänsli · Aral I. Okay · Fukun Chen · Hüseyin Kozlu · Fırat Şengün

Abstract The Alanya Massif, which is located to the south of central Taurides in Turkey, presents a typical nappe pile consisting of thrust sheets with contrasting metamorphic histories. In two thrust sheets, Sugözü and Gündoğmuş nappes, HP metamorphism under eclogite (550–567 °C/14–18 kbar) and blueschist facies (435–480 °C/11–13 kbar) conditions have been recognized, respectively. Whereas the rest of the Massif underwent MP metamorphism under greenschist to amphibolite facies (525–555 °C/6.5–7.5 kbar) conditions. Eclogite facies metamorphism in Sugözü nappe, which consists of homogeneous garnet–glaucophane–phengite schists with eclogite lenses is dated at 84.8 ± 0.8, 84.7 ± 1.5 and 82 ± 3 Ma (Santonian–Campanian) by $^{40}Ar/^{39}Ar$ phengite, U/Pb zircon and rutile dating methods, respectively. Similarly, phengites in Gündoğmuş nappe representing an accretionary complex yield 82–80 Ma (Campanian) ages for blueschist facies metamorphism. During the exhumation, the retrograde overprint of the HP units under greenschist–amphibolite facies conditions and tectonic juxtaposition with the Barrovian units occurred during Campanian (75–78 Ma). Petrological and geochronological data clearly indicate a similar Late Cretaceous tectonometamorphic evolution for both Alanya (84–75 Ma) and Bitlis (84–72 Ma) Massifs. They form part of a single continental sliver (*Alanya–Bitlis microcontinent*), which was rifted from the southern part of the Anatolide–Tauride platform. The *P–T–t* coherence between two Massifs suggests that both Massifs have been derived from the closure of the same ocean (*Alanya–Bitlis Ocean*) located to the south of the Anatolide–Tauride block by a northward subduction. The boundary separating the autochthonous Tauride platform to the north from both the Alanya and Bitlis Massifs to the south represents a suture zone, *the Pamphylian–Alanya–Bitlis suture*.

Keywords Tauride · Eclogite · Alanya · Blueschist · Metamorphism

M. Çetinkaplan (✉) · O. Candan · O. E. Koralay
Department of Geological Engineering, Dokuz Eylül University, 35160 Buca-İzmir, Turkey
e-mail: mete.cetinkaplan@deu.edu.tr

A. Pourteau · R. Oberhänsli
Institut für Geowissenschaften, Universitat Potsdam, Postfach 601553, 14415 Potsdam, Germany

A. I. Okay
Eurasian Institute of Earth Sciences, Technical University of Istanbul, Ayazağa, 80626 Istanbul, Turkey

F. Chen
Chinese Academy of Sciences Key Laboratory of Crust-Mantle Material and Environment, University of Science and Technology of China, Hefei 230026, China

H. Kozlu
Turkish Petroleum Corporation (TPAO), Ankara, Turkey

F. Şengün
Department of Geological Engineering, Çanakkale Onsekiz Mart University, 17020 Çanakkale, Turkey

Introduction

Turkey is made up of large number of amalgamated continental domains, which are separated by mainly E–W-trending suture zones representing the closure site of several Neotethyan oceanic branches. This tectonic mosaic is

the result of successive rifting and oceanisation along the northern margin of Gondwana, northward drifting of the separated continental blocks and, finally, continental collision between Gondwana and Laurasia due to the closure of these multiple oceanic branches of the Tethyan realm during late Paleozoic, early Mesozoic and Late Cretaceous to Tertiary times (Okay et al. 2006; Robertson 2004; Robertson et al. 2013; Stampli and Borel 2002; Şengör and Yılmaz 1981). Within this general tectonic framework, the İzmir–Ankara Suture Zone, formed by the closure of the northern branch of the Neotethys Ocean in Late Cretaceous–Eocene (Candan et al. 2005; Okay and Tüysüz 1999; Okay et al. 2001; Pourteau et al. 2013; Rolland et al. 2009), separates Turkey into two main tectonic units (Ketin 1966; Okay and Tüysüz 1999), the Pontides (Sakarya Zone, Istanbul Zone, Stranja Massif) to the north and the Taurides and their metamorphic equivalents, the Anatolides (Tavşanlı Zone, Afyon Zone, Menderes Massif and Lycian Nappes) to the south. In addition, in SE Anatolia, the Bitlis–Zagros suture zone represents the closure of the southern Neotethys Ocean and collision of the Arabian Plate with the Anatolides–Taurides during Miocene (Parlak et al. 2009; Şengör and Yılmaz 1981; Yılmaz 1993). Taurides and their metamorphic equivalents, Anatolides, show a Gondwanian affinity. The Anatolides–Taurides with common Paleozoic–Early Triassic stratigraphy were rifted off from Gondwana as an isolated block by the opening of the northern and southern branches of the Neotethys Ocean in the Triassic (Göncüoğlu et al. 2003; Okay et al. 1996, 2006) or Jurassic (Şengör et al. 1980, 1985). Based on the primary depositional environments and sedimentary facies characteristics, the Anatolide–Tauride block is divided into several units: these are from south to north, the Alanya, Antalya, Geyik Dağı, Aladağ and Bozkır units (Özgül 1976, 1983).

Within this general tectonic framework, the Alanya Massif is assumed to derive from the Alanya unit as a consequence of Late Cretaceous subduction and associated polyphase metamorphism. The existence of well-preserved eclogite and blueschists in the Alanya Massif has been documented first time by Okay and Özgül (1984) and Okay (1989). In these papers, based on the general geological evidence, a possible Late Cretaceous, Turonian, age was assumed for the high-P metamorphism (Okay and Özgül 1984). More recently, in the Bitlis Massif in the southeastern Anatolia Late Cretaceous eclogites in the basement series and blueschists characterized by the presence of carpholite and glaucophane in the Mesozoic sequence have been discovered (Oberhänsli et al. 2010, 2011). A possible correlation in terms of general geological characteristics between Alanya Massif and Bitlis Massif has been suggested in some papers (Özgül 1976; Çetinkaplan et al. 2011; Oberhänsli et al. 2010). Here, we report the first geochronological data on the HP metamorphism and

following Barrovian-type overprint in the Alanya Massif. We also focus on the Late Cretaceous subduction history of the Alanya Massif and discuss a possible correlation of the geodynamic setting between Alanya and Bitlis Massifs in terms of the Late Cretaceous evolution of the oceanic branches in the Eastern Mediterranean region.

Geology of the Alanya Massif

The Alanya Massif presents a typical nappe pile consisting of thrust sheets with contrasting metamorphic histories. Although the great majority of the Massif was affected by Barrovian-type metamorphism, evidence for HP metamorphism was documented from two localities: in the regions of Alanya (Fig. 1a, b) and Gündoğmuş (Figs. 1a, 2) (Şengün et al. 1978; Okay 1986). The tectonic architecture of the Gündoğmuş region has been regarded as an accretionary complex that was metamorphosed under blueschist facies conditions during the Late Cretaceous. In the Alanya region, the glaucophane- and garnet-bearing phengite schists that contain numerous eclogite lenses exhibit a coherent succession of psammitic to pelitic sedimentary rocks with thin black quartz arenite interlayers.

The Alanya Massif is tectonically underlain by the unmetamorphosed sedimentary sequence of the Antalya Unit (Fig. 1a, b). The Alanya Massif, the Antalya Unit as well as the Taurides, to the north, are unconformably overlain by Late Paleocene–Eocene sedimentary rocks that postdate the exhumation of the metamorphic rocks (Özgül 1976; Demirtaşlı 1983; Işık and Tekeli 1995). During the Lutetian, the Alanya Massif was thrust northward over the autochthonous Tauride platform (Geyik Dağı Unit), and then overthrust from the north by an allochthonous Tauride unit (Aladağ Unit) (Fig. 1b). Therefore, present-day tectonic contacts with the Taurides are related to Eocene tectonics, whereas the metamorphic history of the Alanya Massif carries crucial information on the older history of the Taurides.

Alanya region

In general, this region is made up of two tectonic units, the unmetamorphosed Antalya unit and tectonically overlying Alanya Massif (Fig. 1b). The Antalya unit crops out in a tectonic window and exhibits a coherent but highly deformed sedimentary sequence (Özgül 1976; Okay and Özgül 1984). In the study area, it is composed of platform-type Permian limestone overlain by thinly bedded Scythian carbonate. These are overlain by the Triassic deep-marine sediments, radiolarian cherts and pelagic limestones, with rare basaltic tuff horizons. They pass upwards to Carnian silisiclastic turbidites consisting of more than 300 m-thick
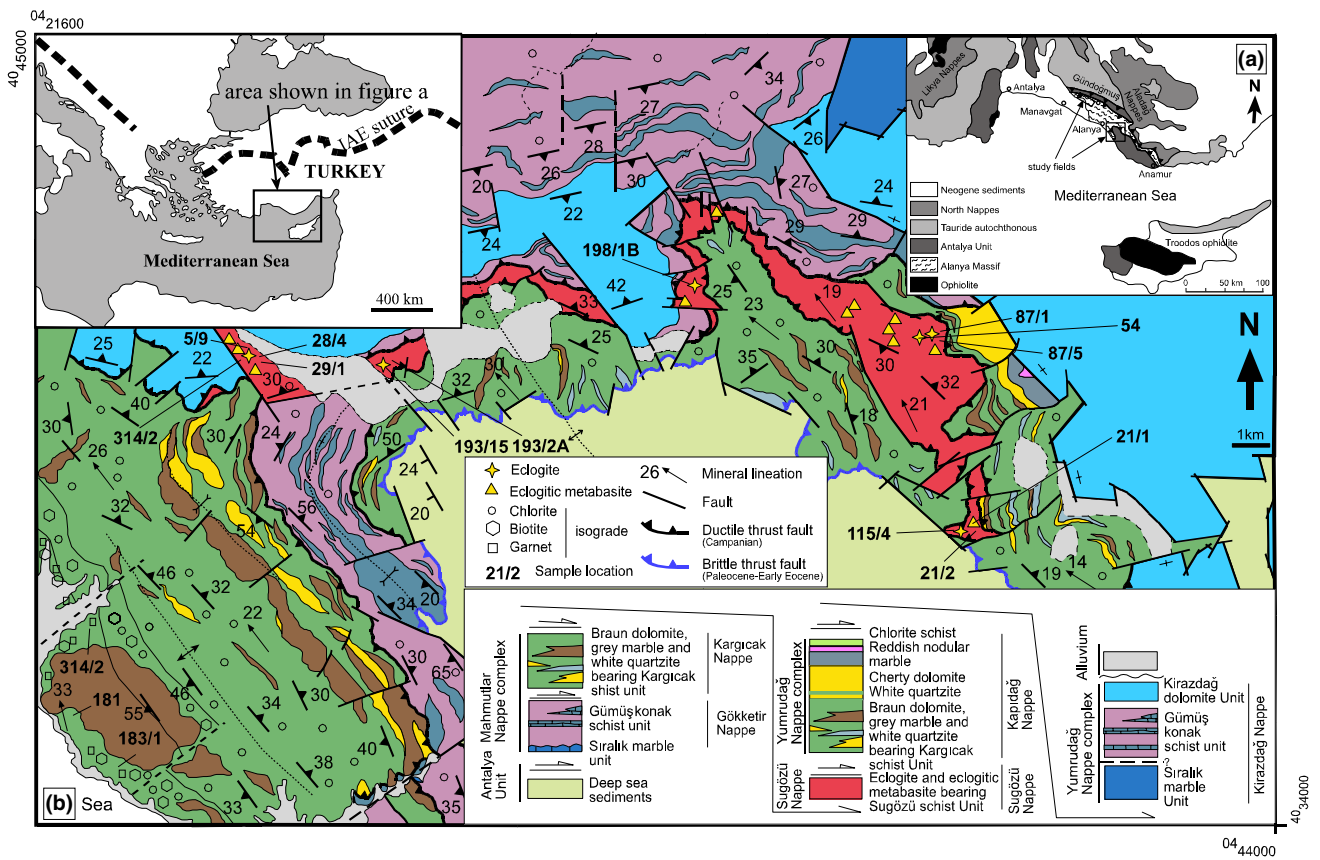
Fig. 1 **a** Generalized tectonic map of the middle Tauride showing the major tectonic units (after Okay 1986), **b** geological map of the Alanya area
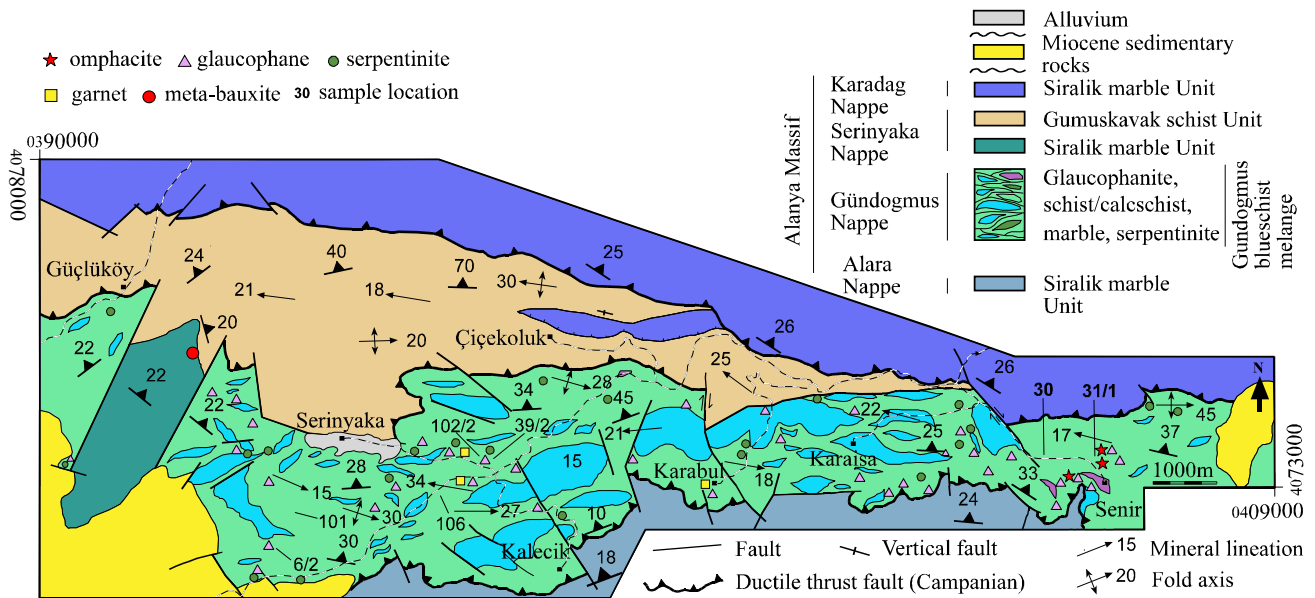

Fig. 2 Geological map of the Gündoğmuş area

interbedded sandstone and mudstone. At the uppermost stratigraphic levels, this intercalation contains reworked meter-to-km-sized olistoliths of gray to black Permian limestone.

The metamorphic rocks of the Alanya Massif consist of the Mahmutlar and Yumrudağ nappe complexes (at lower and upper structural positions, respectively), which have experienced Barrovian-type MP/LT, and the intermediate Suğözü nappe, which was affected by the blueschist facies to eclogite facies conditions (Fig. 1b, Okay and Özgül 1984). The Mahmutlar nappe has a maximum thickness of 900 m. It is made up of two tectonic subunits, from bottom to top, the Gökketir and Kargıcak nappes. The Gökketir nappe consists of Upper Permian marbles with rarely preserved *Mizzia* fossils and conformably overlying intercalations of multicolored chlorite schist, marble and calcschist that are probably lower Triassic in age. In contrast, the Kargıcak nappe is probably Infracambrian in age; it consists predominantly of mica schist, brownish metadolomite, white metaquartzite and gray marble. A well-developed schistosity is ubiquitous in the metaclastics. In the metaclastic sequence, the chlorite, biotite and garnet isogrades define a NE-to-SW progressive increase in metamorphic grade, within the greenschist facies (Okay 1989).

The Suğözü nappe can be followed over 30 km laterally and has a variable thickness of 50–1,000 m. It is dominantly composed of homogeneous garnet–glaucophane–phengite schists of inferred Infracambrian protoliths age. Schists are composed of conspicuous reddish garnet crystals up to 5 mm in size in a phengite-rich matrix (Fig. 3a). Black colored quartzite levels, up to 20 cm thick, are interlayered with schists. Dark blue glaucophane occurs as parallel-aligned prismatic crystals up to 1 cm long, defining the pronounced mineral lineation of the schists. Eclogite and eclogitic metabasite are observed in minor amount (ca. 3 % of the Suğözü Nappe), as layers with maximum 50 cm in thickness and more commonly as boudin reaching up to 4 m in length. Eclogite exhibits a massive to weakly foliated structure and contains 2–3 mm garnet crystals in a dark green groundmass of predominantly omphacite and minor clinozoisite (Fig. 3c). More common eclogitic metabasite contains distinctively higher modes of glaucophane. Due to retrogression at the edges of the eclogitic lenses as well as along crosscutting shear bands, eclogite was transformed partly to completely into retrograde blueschist facies to greenschist facies rocks, such as glaucophanite, epidote–amphibolite, greenschist and all possible intermediates. It occurs as a well-preserved HP tectonic slice between the underlying Mahmutlar and overlying Yumrudağ nappe complexes. The mylonitic-to-ultramylonitic top and basal shear zones of the Suğözü Nappe are marked, in quartz-rich lithologies, by flattened and elongated quartz aggregates separated by planar minerals and, in micaschists, by

phyllonites. Up to 5 m away from the shear zones, garnet and glaucophane are completely to partly replaced by chlorite, representing tectonic juxtaposition and deformation under greenschist facies conditions.

The uppermost, Yumrudağ nappe complex is characterized by lower greenschist facies metamorphism. It is divided into three thrust sheets, from bottom to top, the Kapıkaya, Sıralık and Kiraz Dağ nappes. The Kapıkaya nappe constitutes a coherent metasedimentary sequence of, from bottom to top, chlorite–mica schist (15 m), pink to white metaquartz arenite (20 m), cherty dolomite (2 m), pink–green nodular marble (3 m) and homogeneous chlorite schist with thin nodular marble interlayers at the lower levels (>200 m). This clastic–carbonate sequence can be correlated with typical Infracambrian–Cambro–Ordovician units of the Taurides, which can be traced more than 600 km from eastern to western Anatolia. The Sıralık nappe consists predominantly of strongly folded and moderate to thickly bedded platform-type Upper Permian black marble. The Kiraz Dağ nappe is composed of an intercalation (30–100 m thick) of chlorite–albite schist, yellow dolomite and gray marble of probably Early Triassic age that grades upwards into homogeneous platform-type gray dolomitic marbles, up to 400 m thick, possibly Jurassic in age.

Gündoğmuş region

In this region, four nappes are distinguished (Fig. 2). They are from bottom to top the Alara, Gündoğmuş, Serinyaka and Karadağ nappes. The nappe contains well-preserved evidence for HP/LT metamorphism in the blueschist facies with a strong greenschist facies overprint, whereas the other units have experienced a single metamorphic event in the lower greenschist facies. The nappe pile in the region is unconformably covered by unmetamorphosed Middle Miocene marls (Şenel et al. 1999). Lower Miocene conglomerates northeast of Antalya contain clasts of blueschists (Monod et al. 2006).

The Alara and Karadağ nappes both derived from gray to black, bituminous Upper Permian platform-type marble with scarce chert nodules in the upper levels. The Gündoğmuş nappe consists of tectonic slices of different lithologies and is regarded as an accretionary complex, which underwent blueschist facies metamorphism. The Gündoğmuş nappe is predominantly (>85 %) composed of massive neritic marble and chlorite-bearing calcschist. Other lithologies are pseudo-aragonite marble (5 %), greenschist (lenses up to 200 m in length—4 %), metamorphic serpentinite (2 %), garnet–epidote–glaucophanite (1 %), epidote–glaucophanite (1 %), glaucophane–metachert (1 %), garnet–glaucophanite (1 %), phengite–schist and chloritoid–phengite–schist. Epidote glaucophanites up to 15 × 100 m in size form the dominant high-P rocks of the accretionary complex. Additionally,
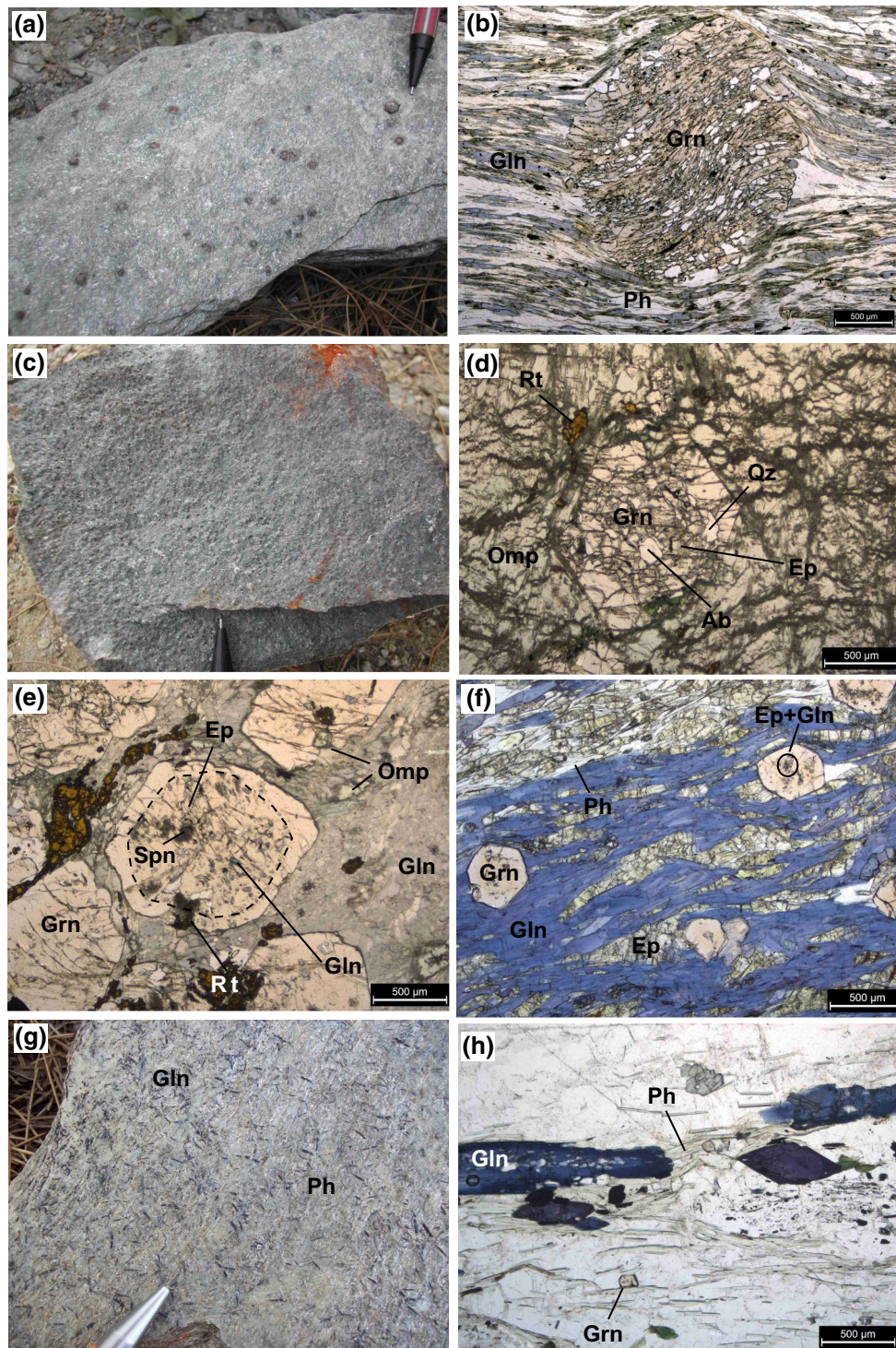
Fig. 3 **a** Garnet–glaucophane–phengite schist from Sugözü Nappe, **b** syn-tectonic garnet in garnet–glaucophane–phengite schist, **c** eclog-ite boulder in Sugözü Nappe, **d** photomicrograph of eclogite; garnet core with albite, epidote and quartz inclusions (sample 87/1), **e** pho-tomicrograph of eclogitic metabasite; garnet core with sphene (*Spn*), epidote (*Ep*) and glaucophane (*Gln*) inclusions (blueschist facies) and garnet rim with rutile (*Rt*) and omphacite (*Omp*) inclusions (eclogite facies), **f** photomicrograph of garnet–epidote glaucophanite, **g** glau-cophane–quartz schist, **h** photomicrograph of glaucophane–quartz schist

garnet–epidote glaucophanite lenses with a maximum size of 3×2 m have been identified at five locations. Glaucophane–bearing metachert (Fig. 3g) up to 1×2 m in size occurs as blocks embedded in a matrix. The upper and lower contacts of Gündoğmuş nappe are ductile thrust faults indicating tectonic juxtaposition of the thrust sheets under lower greenschist facies conditions. The Serinyaka nappe starts with gray to black homogenous marble probably Late Permian in age with a thickness of 300–500 m, with emery lenses in the uppermost levels. These marbles are overlain unconformably by an intercalation of chlorite–muscovite schist, calcschist and dark gray marble of probable Early Triassic age.

Petrography and mineral chemistry

Alanya region

Sugözü Nappe

This nappe is made up of HP/LT metamorphic rocks such as garnet–glaucophane–phengite schist, eclogite and eclogitic metabasites (Fig. 1b). The eclogite facies assemblage omphacite + garnet + rutile is well preserved in the undeformed cores of the eclogitic lenses (Okay 1989). Elsewhere, the peak assemblage in both eclogites and host rocks was retrogressed into blueschist facies and, finally, greenschist facies assemblages.

The initial eclogite facies assemblage of the host rocks of the eclogites was highly obliterated by the blueschist to greenschist overprint. The mineral assemblage in garnet–glaucophane–phengite schists is garnet, glaucophane, phengite, sphene, calcite, quartz, albite and opaque oxides (Table 1). Syntectonic garnet porphyroblasts, 1–5 mm across, contain inclusions of glaucophane, zoisite, sphene and quartz. The lineation of the inclusions in the porphyroblasts is parallel to the foliation of the matrix, which is defined by the preferred orientation of glaucophane and phengite (Fig. 3b). Garnets in the garnet–glaucophane–phengite schists are essentially almandine–grossular–spessartine solid solutions with minor pyrope member ($Alm_{31–62}$, $Grs_{24–29}$, $Sps_{7–41}$, $Prp_{2–6}$; mol%) (Fig. 4a; Table 2). These garnets exhibit minor single-stage growth zoning with a slight increase in Mg and a decrease in Ca and Mn toward the rim (Fig. 5a). Na-amphiboles are glaucophane in composition and their X_{Mg} ($=Mg/(Mg + Fe^{2+})$) ratio ranges between 0.56 and 0.68 (Fig. 6a; Table 3). In well-preserved samples, phengite with 3.42–3.54 Si^{4+} p.f.u. (Fig. 7) occurs as 0.1–1 mm grains associated with paragonite (Table 4). Na content in paragonites varies between 0.48 and 0.56 p.f.u. The maximum K value of paragonite is 0.07 p.f.u. Greenschist facies overprint during the final stage of retrogression is defined by the replacement of garnet and

glaucophane by chlorite and low-Si content (3.10–3.14 Si^{4+} p.f.u.) in white mica. The chlorite of this stage is ripidolite in composition (Table 5). Anorthite content of the plagioclases are between 0.07 and 0.10 p.f.u (Table 8).

Well-preserved eclogite has a simple mineral assemblage consisting of garnet and omphacite with minor accessory phases of rutile, clinozoisite and opaque oxide (Table 1). Their texture ranges from granoblastic to porphyroblastic. Garnet porphyroblasts ($Alm_{58–69}$, $Grs_{19–35}$, $Sps_{1–10}$, $Prp_{4–12}$; mol%) exhibit minor growth zoning with a slight increase in Ca toward the rim (Figs. 4b, 5b). Garnet show pronounced textural zoning, which is marked by a core with albite, epidote, sphene and quartz inclusions and an inclusion poor rim (Fig. 3d). Based on the apparent lack of albite and sphene in the matrix, the inclusion assemblage in the core can be interpreted to represent evidence of a pre-eclogitic low-pressure stage during the prograde evolution of these metabasalts. Clinopyroxene compositional range is $Jd_{40–52}$ (Fig. 8) Mg = 0.28–0.43 and Al^{VI} = 0.39–0.52 p.f.u. (Table 6). Omphacite was consumed by simplectite intergrowth of albite (An: 0.01–0.02 p.f.u, Table 8) and diopside during the retrograde stage. Barroisite grew along shear planes in micro- or macroscale. Influx of H_2O-rich fluids along the shear zones caused retrogression from blueschist facies to greenschist facies conditions. Barroisite was in turn consumed by Ca-amphiboles of edenite–hastingsite composition (Fig. 6b, c). Replacement of garnet by the assemblage epidote + albite + chlorite and Ca-amphibole by chlorite mark the final stage of retrogression under greenschist facies conditions.

Eclogitic metabasites differ from eclogite by the high modes of glaucophane (Fig. 6a). Garnet and glaucophane may represent up to 80 % of the mode. The peak mineral assemblage is omphacite, garnet, rutile, glaucophane, clinozoisite, phengite, quartz and magnetite (Table 1). Idioblastic garnet porphryoblasts ($Alm_{55–68}$, $Grs_{22–30}$, $Sps_{1–14}$, $Prp_{4–10}$) show both compositional (Fig. 4b; Table 2) and textural zoning. End-member profiles (Fig. 5c) and inclusion assemblage in garnets indicate two stages of continuous growth. Inclusions in garnet core are glaucophane, sphene, epidote and quartz (Fig. 3e). These inclusions show a pronounced orientation reflecting an early foliation witnessing a prograde blueschist facies stage. This internal fabric transects the foliation of the matrix. Garnet rims contain inclusions of omphacite, glaucophane and rutile, which show continuity with the foliation of the matrix. This inclusion pattern clearly reveals that the prograde blueschist facies inclusions can be found in the eclogitic metabasites. Sodic pyroxenes in eclogitic metabasites are omphacite ($Jd_{34–48}$) in composition (Fig. 8; Table 6). Mg and Al^{VI} contents of the omphacite range between 0.30–0.41 and 0.34–0.48 p.f.u., respectively. Omphacite is replaced partly to completely by barroisite and Ca-amphibole.

Table 1 Mineral assemblage and coordinates of the samples

	Sample no.	Omp	Grt	Gln	Na–Ca Amp	Ca Amp	Ep group	Cld	White mica	Pg	Bt	Chl	Pl	Rt	Spn	Cal	Qz	Coordinate (36S)
*1	21/1	X	X	X	X									X	X		X	0439677 4037431
*1	314/2	X	X	X	X				X					X	X		X	0425389 4041056
*1	5/9	X	X	X	X		X							X	X		X	0425271 4041636
*2	87/1	X	X				X							X	X		X	0439275 4041301
*2	193/15	X	X						X				X	X	X		X	0428559 4040807
*2	115/4	X	X						X				X	X	X			0440521 4037507
*2	193/2A	X	X		X									X	X			0428553 4040807
*2	198/1B	X	X		X		X		X					X	X			0434478 4042412
*2	193/5	X	X		X	X	X							X	X			0402859 4040807
*2	79/2	X	X		X		X		X					X	X			0438478 4041670
*3	29/1		X	X	X	X			X	X		X	X				X	0425341 4041594
*3	28/4		X		X	X			X	X		X	X				X	0425272 4041634
*4	87/5		X	X					X			X	X				X	0439275 4041301
*4	21/2		X	X					X	X	X	X	X		X	X	X	0439642 4037394
*4	54		X	X	X				X	X	X	X	X				X	0439301 4041283
*5	181		X						X	X	X	X	X				X	0422129 4034152
*5	183/1		X						X	X	X	X	X				X	0422642 4033719
*6	341/5		X						X	X		X	X				X	0422326 4035538
*7	6/2		X	X			X		X			X	X					0393529 4072141
*7	106		X	X	X	X	X					X						0396196 4072985

Table 1 continued

Sample no.	Omp	Grt	Gln	Na–Ca Amp	Ca Amp	Ep group	Cld	White mica	Pg	Bt	Chl	Pl	Rt	Spn	Cal	Qz	Coordinate (36S)
*8 101						X	X	X			X	X				X	0393728 4072425
*9 39/2			X			X		X									0396655 4073132
*9 30		X	X			X		X			X	X				X	0405751 4073424
*10 31/1		X	X			X		X									0406437 4073069
*11 102/2				X	X			X			X	X					0396627 4073321

Sugözü Nappe (*1: eclogitic metabasite,*2: eclogite,*3: garnet–amphibolite,*4: garnet–glaucophane–phengite schist)

Kargıcak Nappe (*5: garnet–biotite–chlorite schist;*6: garnet–biotite schist)

Gündoğmuş Nappe (*7: garnet–epidote glaucophanite,*8: Chloritoid–phengite schist,*9: glaucophane–quartz schist)

*10: phengite–epidote glaucophanite,*11: amphibolite)

Omp omphacite, *Grt* garnet, *Gln* glaucophane, *Amp* amphibole, *Ep* epidote, *Cld* chloritoid, *Pg* paragonite, *Bt* biotite, *Chl* chlorite, *Pl* plagioclase, *Rt* rutile, *Spn* sphene, *Cal* calcite, *Qz* quartz

Mahmutlar Nappe complex

In the Gökketir nappe (lower nappe unit of the Mahmutlar Nappe complex), the mineral assemblage in the chlorite schists is chlorite (X_{Mg} = 0.49–0.51), albite, muscovite and quartz (Tables 1, 5). In the Kargıcak Nappe, the prograde metamorphic sequence is marked by a regular decrease in the modal amounts of chlorite (X_{Mg} = 0.58–0.59) and albite (An = 0.02) and increase in biotite (X_{Mg} = 0.55–0.59) (Table 4). End-member profiles of the garnet porphyroblasts (Fig. 5d) in garnet–biotite–chlorite schists ($Alm_{59–67}$, $Grs_{16–22}$, $Sps_{5–15}$, $Prp_{5–8}$, mol%) (Fig. 4c) show a single-stage growth zoning. White mica Si^{4+} content ranges between 3.05 and 3.22 p.f.u. (Fig. 7).

Gündoğmuş region

In the Gündoğmuş nappe, blueschist metabasite is composed of garnet, glaucophane, epidote, phengite, albite, sphene and chlorite (Table 1). Garnet forms idiomorphic crystals 0.25–1 mm in size. It contains epidote, glaucophane and sphene inclusions, which are indicative of growth under blueschist facies conditions (Fig. 3f). Garnet are essentially almandine–spessartine–grossular solid solution with minor pyrope components ($Alm_{31–62}$, $Grs_{22–25}$, $Sps_{7–41}$, $Prp_{2–6}$) (Fig. 4d; Table 2). Core to rim zoning consists in a decrease in Mn mainly in favor of Fe (Fig. 5e). Grossular and pyrope components do only slightly increase from core to rim. Na-amphibole, which generally forms idioblastic crystals, is glaucophane with X_{Mg} = 0.59–0.68 and exhibits no significant zoning (Fig. 6a; Table 3). Phengite (Si^{4+} = 3.46–3.58 p.f.u.) (Table 4), which defines the main foliation, reaches up to 600 μm in size. Phengite plots slightly above $Si(Fe^{2+}, Mg)Al_{-2}$ line, suggesting the presence of low amounts of Fe^{3+} (Fig. 7). Epidote shows a slight compositional zoning, which is defined by Fe^{3+}-rich cores ($Ps(=Fe^{3+}/Fe^{3+}Al_{-2})$ 0.36–0.37) and Al-rich rims (Ps = 0.33) (Table 7). The HP/LT metamorphic minerals are generally well preserved in the glaucophanites, in which the retrograde overprint under greenschist facies conditions is restricted only to the partial replacement of garnet by chlorite (X_{Mg} = 0.49) (Table 5). Plagioclases are albite in composition (Table 8) and their anorthite content is 0.05 p.f.u.

Glaucophane-bearing quartzite presents a lineation marked by parallel-aligned phengite and glaucophane (0.5 cm in length) crystals (Fig. 3g). These metacherts are made of quartz, garnet, glaucophane, chlorite, phengite and albite (Table 1). Garnet, occurring as small idioblastic crystals <100 μm in size, is rich in spessartine ($Alm_{8–12}$, $Grs_{10–14}$, $Sps_{75–76}$, $Prp_{1–2}$, mol%) (Table 2). Although all Na-amphibole plots in the glaucophane field (Fig. 6a), it is widely zoned from core to rim with content in Al^{VI} decreasing from 0.99–1.09 to 0.74–0.89 and X_{Mg} values increasing

Fig. 4 Chemical composition of garnet in the (alm + sps)–prp–grs triangular diagram for **a** garnet–glaucophane–phengite schist, **b** eclogitic metabasite and eclogite, **c** garnet–biotite schist, **d** blueschist metabasite
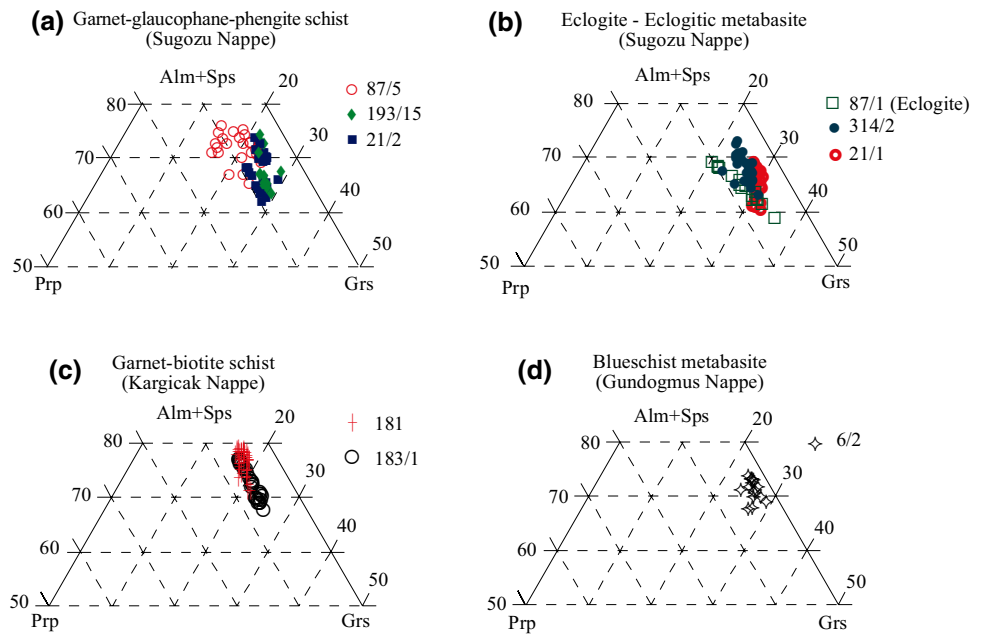
from 0.56–0.57 to 0.74–0.89 (Table 3). Si^{4+} content of phengite ranges between 3.51 and 3.59 p.f.u. (Table 4). Similar to glaucophane, phengite shows a weak compositional zoning of Si^{4+} content, which decreases from 3.57 to 3.51 p.f.u. toward the rim. The retrograde overprint under greenschist facies conditions in these rocks is defined by the replacement of glaucophane by chlorite. The mineral assemblage in chloritoid–phengite schists is chloritoid, phengite, zoisite, chloride, albite and quartz. X_{Mg} ratio of chloritods is between 0.04 and 0.07 (Table 9). The compositional range of phengite (Si^{4+}) and chloride (X_{Mg}) is 3.36–3.42 p.f.u and 0.16–0.18, respectively. Anorthite content of the plagioclase is 0.05 p.f.u. (Table 8).

P–T estimations

Conventional geothermobarometric calibrations based on the Fe/Mg exchange and mass-transfer reactions were applied to eclogitic metabasite (21/1; 314/2), eclogite (5/9; 87/1), garnet–amphibolite (29/1), garnet–glaucophane–phengite schist (87/5; 21/2) and garnet–biotite schist (181; 183/1), garnet–epidote glaucophanite (6/2; 106) and chloritoid–phengite schist (101) (Table 1). P–T estimates are compiled in Table 10. Additionally, P–T conditions for samples 314/2, 21/2, 183/1 and 101 are estimated using THERIAK–DOMINO software package (De Capitani and Brown 1987; De Capitani and Petrakakis 2010), updated JAN92.RGB database of Berman (1988), glaucophane data of Holland and Powell (1998) and the alumino-celadonite data from Massonne and Szpurka (1997).

Alanya region

Sugözü Nappe

The calibration of Graham and Powell (1984) has been applied to garnet–amphibole pairs of eclogitic metabasite (314/2, 21/1) and garnet–amphibolite (29/1). Garnet in sample 314/2 displays textural zoning represented by inclusion-rich garnet cores (glaucophane, zoisite and sphene inclusions of prograde blueschist stage) and rim with less inclusion (omphacite, glaucophane and rutile assemblage of eclogitic stage). In sample 314/2, local pairs of glaucophane inclusions and surrounding garnet yield temperatures of 457–488 °C for the prograde blueschist facies assemblage in garnet cores (at 12 kbar) and 503–509 °C for the eclogitic assemblage in garnet rims (at 16 kbar). Garnet–amphibole pairs thus depict a slight temperature increase consistent with petrographic observations. In sample 21/1, although garnet display no pronounced textural zoning, a similar temperature increase was obtained: from 450 °C in cores to 508 °C in rims (at 16 kbar). In garnet–amphibolite sample 29/1 collected from the rind of an eclogite body in the Sugözü nappe, pairs of garnet rim and Na–Ca-amphibole core yielded 483–533 °C (at 7 kbar) and pairs of garnet rims and Na–Ca-amphibole rim yielded 397–421 °C (at 7 kbar). Rim temperature results indicate an isothermal decompression during the retrogression (Table 10).

Six garnet–clinopyroxene geothermometry calibrations were applied to eclogitic metabasite (21/1, 314/2) and eclogite (87/1) (Table 10). These calibrations yield temperatures of 467–571 °C at a pressure of 16 kbar were

Table 2 Selected microprobe analyses of garnet (sample descriptions are given by Table 1)

Sample	21/1 Rim	21/1 Core	314/2 Rim	314/2 Rim	314/2 Core	314/2 Core	87/1 Rim	87/1 Core	21/2 Rim	21/2 Core	29/1 Rim	29/1 Core	87/5 Rim	87/5 Core	183/1 Rim	183/1 Core	181 Rim	181 Core	106 Rim	106 Core
SiO_2	37.76	38.46	37.63	38.64	37.99	38.61	38.60	38.36	38.69	38.37	38.44	38.81	38.96	37.75	37.65	37.14	37.46	37.11	37.26	37.45
TiO_2	0.06	0.12	0.06	0.14	0.20	0.07	0.10	0.12	0.08	0.14	0.14	0.11	0.10	0.16	0.17	0.11	0.07	0.16	0.09	0.15
Al_2O_3	20.53	19.80	20.59	19.92	20.15	19.91	20.77	20.62	20.58	19.48	20.52	20.59	20.42	19.96	21.53	21.50	21.63	21.26	21.61	21.53
FeO	30.07	27.88	29.72	30.09	29.56	31.00	27.49	27.90	29.49	30.68	28.29	28.25	31.32	29.96	29.79	27.67	30.16	27.45	30.16	28.28
MnO	0.41	3.54	0.64	0.62	1.29	0.77	1.06	3.32	0.59	0.77	2.38	2.21	0.34	1.63	1.32	7.00	1.34	6.79	1.25	2.22
MgO	2.22	1.39	2.40	2.06	1.08	1.62	1.90	1.00	2.28	1.42	3.96	3.06	3.03	1.53	1.88	1.59	2.04	1.34	1.42	0.87
CaO	9.07	8.91	8.91	8.94	10.68	8.73	10.09	8.90	8.51	9.60	6.82	7.05	6.12	8.92	8.36	5.68	7.71	6.61	8.42	10.36
Na_2O	0.04	0.02	0.03	0.00	0.02	0.01	0.03	0.06	0.04	0.04	0.01	0.03	0.04	0.04	0.02	0.03	0.03	0.07	0.01	0.01
K_2O	0.01	0.00	0.00	0.01	0.00	0.01	0.00	0.00	0.01	0.02	0.01	0.00	0.01	0.02	0.01	0.00	0.02	0.00	0.01	0.01
Cr_2O_3	0.03	0.01	0.03	0.02	0.00	0.00	0.01	0.03	0.00	0.00	0.03	0.04	0.01	0.02	0.00	0.00	0.00	0.00	0.00	0.00
Total	100.18	100.13	100.02	100.42	100.97	100.73	100.04	100.30	100.27	100.53	100.60	100.14	100.34	99.99	100.73	100.72	100.45	100.79	100.21	100.88
Cations per 24 oxygens																				
Si	6.02	6.12	6.01	6.14	6.05	6.14	6.07	6.08	6.06	6.13	6.06	6.07	6.13	6.06	5.93	5.94	5.92	5.94	5.95	5.95
Ti	0.01	0.01	0.01	0.02	0.02	0.01	0.01	0.01	0.01	0.02	0.02	0.01	0.01	0.02	0.02	0.01	0.01	0.02	0.01	0.02
Al	3.86	3.71	3.87	3.73	3.78	3.73	3.85	3.85	3.80	3.67	3.81	3.80	3.79	3.78	4.00	4.05	4.03	4.01	4.07	4.03
$*Fe^{3+}$	0.14	0.17	0.15	0.09	0.19	0.10	0.06	0.02	0.16	0.19	0.13	0.12	0.03	0.15	0.09	0.00	0.09	0.05	0.00	0.02
Fe^{2+}	3.87	3.68	3.82	3.91	3.75	4.03	3.55	3.67	3.96	3.91	3.60	3.58	4.22	3.88	3.84	3.70	3.90	3.63	4.03	3.73
Mn	0.05	0.48	0.09	0.08	0.17	0.10	0.14	0.58	0.08	0.10	0.32	0.29	0.04	0.22	0.31	0.95	0.31	0.92	0.17	0.30
Mg	0.53	0.33	0.57	0.49	0.26	0.38	0.44	0.24	0.53	0.34	0.93	0.95	0.71	0.37	0.44	0.38	0.48	0.32	0.34	0.21
Ca	1.55	1.52	1.52	1.52	1.82	1.49	1.87	1.51	1.43	1.64	1.15	1.18	1.03	1.54	1.41	0.97	1.31	1.13	1.44	1.76
Na	0.01	0.01	0.01	0.00	0.01	0.00	0.01	0.02	0.01	0.01	0.00	0.01	0.01	0.01	0.01	0.01	0.01	0.02	0.00	0.00
K	0.00	0.00	0.00	0.00	0.00	0.00	0.00	0.00	0.00	0.00	0.00	0.00	0.00	0.00	0.00	0.00	0.00	0.00	0.00	0.00
Cr	0.00	0.00	0.00	0.00	0.00	0.00	0.00	0.00	0.00	0.00	0.00	0.01	0.00	0.00	0.00	0.00	0.00	0.00	0.00	0.00
Total	16.04	16.01	16.05	15.98	16.04	15.99	16.00	15.99	16.04	16.02	16.02	16.01	15.97	16.03	16.05	16.02	16.06	16.04	16.01	16.02
Alm (%)	64.46	61.25	63.62	65.10	62.48	67.08	59.13	61.23	66.03	65.23	60.02	59.66	70.25	64.59	63.95	61.68	65.01	60.44	67.43	62.23
Prp (%)	8.79	5.49	9.52	8.14	4.26	6.39	7.40	3.93	8.87	5.63	15.50	15.78	11.83	6.11	7.38	6.30	8.01	5.33	5.64	3.42
Sps (%)	0.91	7.95	1.45	1.40	2.90	1.73	2.36	9.66	1.29	1.73	5.29	4.88	0.75	3.70	5.15	15.80	5.21	15.34	2.82	4.97
Grs (%)	25.84	25.30	25.40	25.36	30.35	24.80	31.11	25.18	23.80	27.40	19.19	19.69	17.17	25.60	23.52	16.22	21.76	18.88	24.11	29.37
*XMg	0.12	0.08	0.13	0.11	0.06	0.09	0.11	0.06	0.12	0.08	0.21	0.21	0.14	0.09	0.10	0.09	0.11	0.08	0.08	0.05
	0.12	0.08	0.13	0.11	0.06	0.09	0.11	0.06	0.12	0.08	0.21	0.21	0.14	0.09	0.10	0.09	0.11	0.08	0.08	0.05

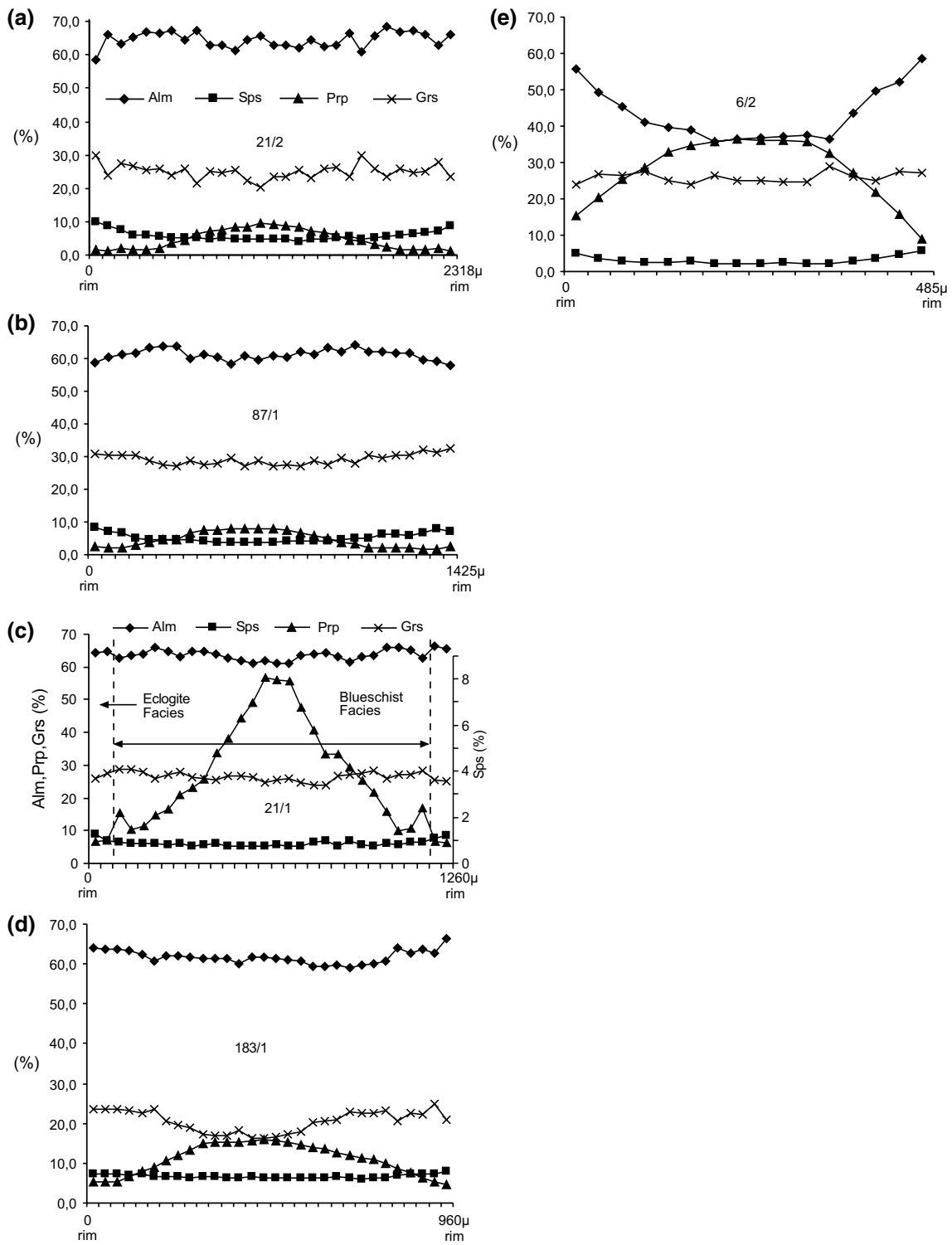*XMg = Mg/Mg + Fe^{2+}, $*Fe^{3+}$ was estimated by charge balance

Fig. 5 Zoning profiles of garnet in samples **a** 21/2, **b** 87/1, **c** 21/1, **d** 183/1, **e** 6/2

obtained for garnet core–omphacite core pairs. The calibrations of Ai (1994) and Krogh Ravna (2000) give estimates (467–498 °C) that are lower by at least 20–30 °C than the other five calibrations (Table 10). For sample 314/2,

temperatures of 498–556 °C were calculated for the eclogite facies peak metamorphic stage. In garnet–glaucophane–phengite schists (87/5, 21/2), the garnet–phengite thermometer of Green and Hellman (1982) provides estimates
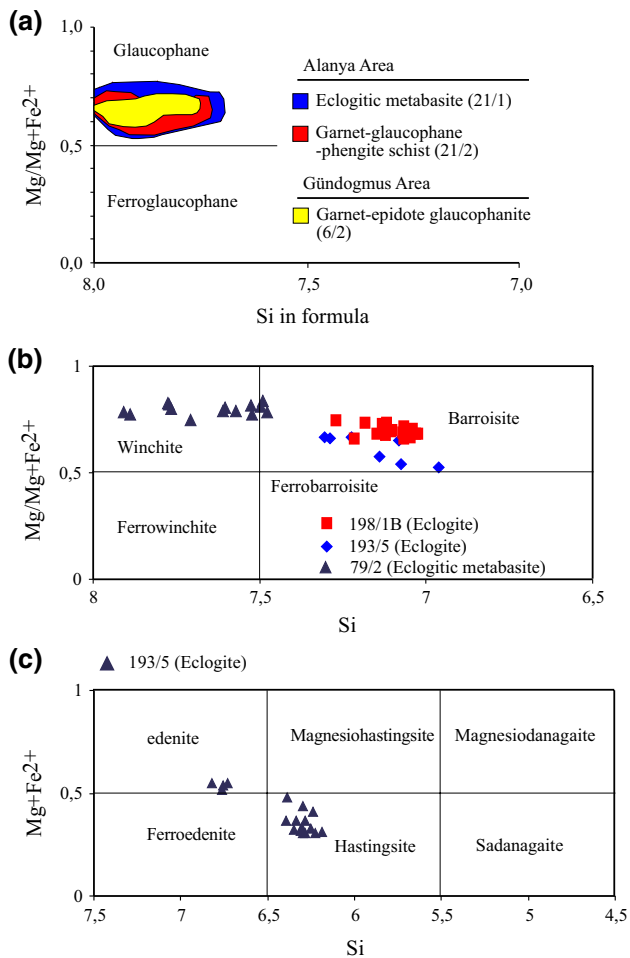
(a)

(b)

(c)

Fig. 6 Compositional plot for **a** Na, **b** Na–Ca, **c** Ca-amphiboles from metabasic and metapelites of Sugözü and Gündoğmuş Nappes using Leake et al. (1997) classification

of 498–538 °C (at 16 kbar) for pairs of phengite inclusions and hosting garnet core (Table 10).

Zr in rutile thermometry based on Zr content of rutile coexisting with zircon and quartz was applied for one eclogitic metabasite sample (5/9). The Zr concentration in rutile is regarded to be mainly temperature controlled (e.g., Zack et al. 2004). Rutile grains from sample 5/9 have Zr content ranging between 94 and 117 ppm, average in 107 ppm. For temperature calculations, Zack et al. (2004), Watson et al. (2006), Ferry and Watson (2007) and Tomkins et al. (2007) calibrations were applied. The calibration of Zack et al. (2004) based on empirical and natural samples gave the temperature of 587 °C. Temperatures calculated by using the calibrations of Watson et al. (2006) which is based on experimental and natural results and Ferry and Watson (2007) which is sensitive to the activity of SiO_2 are 565 and 567 °C, respectively (Table 10). The pressure (18 kbar) estimated by phase equilibrium calculation using Domino/Theriak (de Capitani and Brown 1987)

was used in the equation of Tomkins et al. (2007) incorporated the pressure dependence, and a temperature value of 616 °C was calculated (Table 10).

In the pseudosections for samples 314/2 and 21–2, we have used the intersection of isopleths of the equilibrium assemblages consisting of garnet, glaucophane and omphacite to determine the P–T conditions of the prograde stages of blueschist to eclogite. To calculate the P–T conditions of the blueschist facies metamorphism for sample 314/2 (Fig. 9a, b), the intersection of X_{Mg} isopleths (0.52–0.56) of glaucophane inclusions in garnet core and the X_{Mg} isopleths (0.06–0.09) of garnet core composition are used. They indicate that during the prograde blueschist stage, garnet core was stable in a temperature/pressure range of 460–480 °C/12–13 kbar represented by the stability field of garnet + glaucophane + phengite + zoisite + chlorite + quartz assemblage. X_{Mg} isopleths of garnet rim composition (0.11–0.13) and glaucophane (X_{Mg} = 0.60–0.62) and omphacite (X_{Mg} = 0.70–0.72) occurring in the matrix show that garnet rims were stable at pressure/temperature conditions of 500–550 °C and 14–18 kbar (eclogitic stage) represented by the field of garnet + glaucophane + omphacite + phengite assemblage. Although it can be observed petrographically, the equilibrium field for Na–Ca-amphiboles representing the early stages of retrogression under blueschist facies conditions does not exist in the pseudosections. Barroisite and garnet were consumed by Ca-amphiboles and the assemblage epidote + albite + chlorite, respectively. Realistic P–T estimations (500–550 °C/6–7 kbar), which are consistent well with conventional method can be obtained (Fig. 9b).

In sample 21/2 (Fig. 10), X_{Mg} value of glaucophane ranges from 0.52 to 0.60. The location of $X_{Mg (glau)}$ = 0.6 isopleth represents the upper limit of chlorite and stable glaucophane composition in garnet + glaucophane + phengite + paragonite + quartz field. The pseudosection is contoured for X_{Mg} isopleths for garnet from core to rim (0.08–0.11) and for Si p.f.u. in phengite (Si^{4+} = 3.40–3.42). Isopleth intersections show that syn-tectonic garnet with glaucophane inclusions is stable at 520–560 °C and 13.5–17.5 kbar (eclogite facies). The absence of omphacite in the eclogite facies equilibrium assemblage in the rock should be related to the paragonite stability field under high-pressure conditions.

Kargıcak Nappe: Garnet–biotite and garnet–muscovite Fe/Mg exchange thermometer calibrations given in Table 10 were applied to garnet–biotite schist (181, 183/1). The garnet–biotite calibrations (Table 10) for garnet rim–biotite rim pairs give temperatures of 442–479 and 443–485 °C (at 7 kbar) for samples 181 and 183/1, respectively. Higher values (538–561 °C) are obtained with the garnet–muscovite geothermometer of Green and Hellman (1982) using garnet rim–muscovite rim pairs (Table 10). Because

Table 3 Selected micropyrobe analyses of amphiboles (sample descriptions are given by Table 1)

| Sample	21/1	21/1	21/1	21/1	314/2 (c)	314/2 (c)	314/2 (g)	314/2 (g)	29/1	29/1	87/1	87/1	21/2	21/2	6/2	6/2	106	106	106
SiO_2	58.12	58.63	43.52	41.51	54.43	51.72	52.04	55.96	49.79	49.19	57.43	57.36	57.40	58.24	56.22	56.93	56.13	46.97	48.65
TiO_2	0.06	0.00	0.19	0.27	0.15	0.26	0.32	0.14	0.22	0.23	0.06	0.10	0.03	0.00	0.01	0.01	0.21	0.33	0.21
Al_2O_3	11.38	9.50	11.49	14.39	9.54	12.58	12.11	11.96	10.32	11.04	11.11	11.09	11.09	11.25	6.76	7.86	11.75	12.06	8.23
FeO	11.92	12.09	25.93	23.52	15.17	12.59	12.12	10.88	11.88	12.62	11.69	12.01	13.16	12.31	17.31	15.91	14.41	17.64	18.05
MnO	0.03	0.02	0.22	0.18	0.11	0.06	0.06	0.03	0.07	0.02	0.02	0.01	0.00	0.00	0.14	0.14	0.00	0.07	0.06
MgO	9.34	10.33	2.78	2.58	9.12	9.43	10.27	9.95	12.75	11.86	9.59	9.65	8.74	8.64	9.78	9.59	7.83	8.94	10.92
CaO	0.81	1.01	5.51	5.68	2.86	3.79	3.96	2.76	8.77	9.12	0.82	0.98	0.72	0.44	1.75	1.41	0.47	7.39	8.92
Na_2O	6.96	6.43	5.98	5.97	6.12	6.34	6.19	6.28	3.46	3.24	7.11	6.96	7.35	7.40	6.40	6.69	6.63	4.12	2.87
K_2O	0.04	0.02	0.11	0.39	0.06	0.23	0.26	0.12	0.27	0.33	0.05	0.06	0.02	0.01	0.03	0.03	0.01	0.29	0.20
Cr_2O3	0.01	0.01	0.00	0.01	0.02	0.01	0.00	0.02	0.04	0.03	0.00	0.02	0.00	0.00	0.01	0.00	0.00	0.00	0.00
Total	98.67	98.03	95.74	94.50	97.57	97.01	97.33	98.10	97.54	97.68	97.88	98.24	98.51	98.29	98.41	98.56	97.43	97.81	98.11
Calculated on the basis of 16 cations																			
T: Si	7.91	7.99	6.80	6.55	7.68	7.36	7.35	7.73	7.10	7.06	7.89	7.85	7.89	8.00	7.83	7.88	7.77	6.82	7.03
Al(IV)	0.09	0.01	1.20	1.45	0.32	0.64	0.65	0.27	0.90	0.94	0.11	0.15	0.11	0.00	0.17	0.12	0.23	1.18	0.97
Fe^{3+}	0.00	0.00	0.00	0.00	0.00	0.00	0.00	0.00	0.00	0.00	0.00	0.00	0.00	0.00	0.00	0.00	0.00	0.00	0.00
Ti	0.00	0.00	0.00	0.00	0.00	0.00	0.00	0.00	0.00	0.00	0.00	0.00	0.00	0.00	0.00	0.00	0.00	0.00	0.00
T-Sum	8.00	8.00	8.00	8.00	8.00	8.00	8.00	8.00	8.00	8.00	8.00	8.00	8.00	8.00	8.00	8.00	8.00	8.00	8.00
C: Al(VI)	1.74	1.52	0.91	1.23	1.26	1.47	1.37	1.68	0.84	0.92	1.69	1.64	1.69	1.82	0.94	1.16	1.69	0.88	0.44
Ti	0.01	0.00	0.02	0.03	0.02	0.03	0.03	0.01	0.02	0.02	0.01	0.01	0.00	0.00	0.00	0.00	0.02	0.04	0.02
Fe^{3+}	0.25	0.49	0.56	0.32	0.48	0.17	0.28	0.04	0.32	0.21	0.27	0.34	0.23	0.08	0.98	0.74	0.57	0.72	0.88
Cr	0.00	0.00	0.00	0.00	0.00	0.00	0.00	0.00	0.00	0.00	0.00	0.00	0.00	0.00	0.00	0.00	0.00	0.00	0.00
Mg	1.89	2.10	0.65	0.61	1.92	2.00	2.16	2.05	2.71	2.54	1.96	1.97	1.79	1.77	2.03	1.98	1.62	1.93	2.35
Fe^{2+}	1.10	0.89	2.82	2.78	1.31	1.33	1.15	1.21	1.09	1.31	1.07	1.04	1.28	1.33	1.04	1.11	1.10	1.42	1.30
Mn	0.00	0.00	0.03	0.02	0.01	0.01	0.01	0.00	0.01	0.00	0.00	0.00	0.00	0.00	0.02	0.02	0.00	0.01	0.01
Ca	0.00	0.00	0.00	0.00	0.00	0.00	0.00	0.00	0.00	0.00	0.00	0.00	0.00	0.00	0.00	0.00	0.00	0.00	0.00
C-Sum	5.00	5.00	5.00	5.00	5.00	5.00	5.00	5.00	5.00	5.00	5.00	5.00	5.00	5.00	5.00	5.00	5.00	5.00	5.00
B: Ca	0.12	0.15	0.92	0.96	0.43	0.58	0.60	0.41	1.34	1.40	0.12	0.14	0.11	0.06	0.26	0.21	0.07	1.15	1.38
Na	1.84	1.70	1.08	1.04	1.57	1.42	1.40	1.59	0.66	0.60	1.88	1.85	1.89	1.94	1.73	1.79	1.78	0.85	0.62
B-Sum	1.96	1.85	2.00	2.00	2.00	2.00	2.00	2.00	2.00	2.00	2.00	1.99	2.00	2.00	1.99	2.00	1.85	2.00	2.00
A: Ca	0.00	0.00	0.00	0.00	0.00	0.00	0.00	0.00	0.00	0.00	0.00	0.00	0.00	0.00	0.00	0.00	0.00	0.00	0.00
Na	0.00	0.00	0.73	0.79	0.10	0.33	0.29	0.09	0.30	0.30	0.01	0.00	0.07	0.03	0.00	0.00	0.00	0.31	0.19
K	0.01	0.00	0.02	0.08	0.01	0.04	0.05	0.02	0.05	0.06	0.01	0.01	0.00	0.00	0.01	0.01	0.00	0.05	0.04
A-Sum	0.01	0.00	0.76	0.87	0.12	0.37	0.34	0.11	0.35	0.36	0.02	0.01	0.07	0.04	0.01	0.01	0.04	0.36	0.22
XMg	0.58	0.60	0.16	0.16	0.52	0.57	0.60	0.62	0.71	0.66	0.65	0.66	0.54	0.56	0.50	0.52	0.49	0.47	0.52

c core, *g* ground, Fe^{3+} was estimated by charge balance
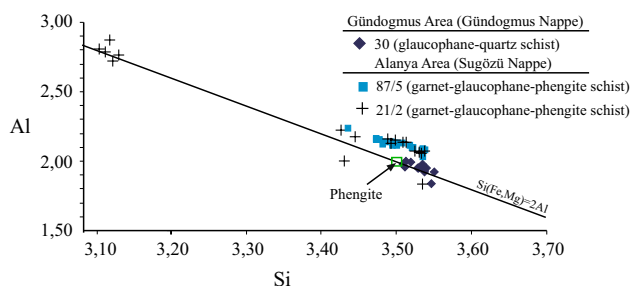
Fig. 7 Phengite compositions plotted in Si versus (Fe + Mg) diyagram. *Line* represents the ideal celadonite subsutition ($Si(Fe^{2+}, Mg) Al_{-2}$)

similar temperature values are inferred from thermodynamic modeling of sample 183/1, an average temperature of about 550 ± 10 °C (7 ± 1 kbar) can be estimated for the garnet isograd of the Kargıcak nappe.

The Fe/Mg exchange geobarometers for the parageneses garnet–aluminosilicate–quartz–plagioclase (GASP; Koziol and Newton 1988), and garnet–plagioclase–muscovite ($Si^{4+} \leq 3.22$ p.f.u)–biotite (GPMB; Hoisch 1991) were used for samples 181 and 183/1. GASP and GPMB (Mg–Fe) calibrations yield 7.7–8.3 kbar and 8.1–8.5 kbar (Mg) and 7.2–7.5 kbar (Fe) for 181 and 183/1, respectively. Because pressure estimates directly are very sensitive to anorthite content of plagioclase (181: An_{26}, 183/1: An_{25}), they are regarded as maximum values. For sample 183/1 (Fig. 11), the assemblage garnet + biotite + chlorite + muscovite + albite + quartz covers narrow equilibrium field in pseudosections. Phengite Si^{4+} (3.20–3.24 p.f.u) isopleths in this field define 525–555 °C and 6.5–7.5 kbar.

On the basis of the results in Alanya area, the *P–T* path shown in Fig. 12 can be constructed for the Sugözü Nappe: prograde blueschist facies stage at 460–480 °C/12–13 kbar, followed by peak in the eclogite facies at 500–567 °C/14–18 kbar and Barrovian overprint at 500–550 °C/6–7 kbar. Barrow facies conditions in Kargıcak Nappe is $T = 525$–555 °C and $P = 6.5$–7.5 kbar. Okay (1989) estimated 510 ± 25 °C and 13.5 ± 1.5 kbar for the peak eclogite facies metamorphism in the Sugözü nappe and the Barrovian metamorphic overprint at 6.5 ± 1.5 kbar.

Gündoğmuş region

Temperature conditions of both blueschist facies metamorphism and greenschist facies overprint in Gündoğmuş area were determined for samples 6/2 and 106. The garnet–phengite geothermometers of Krogh and Raheim (1978) and Green and Hellman (1982) and the garnet–amphibole geothermometer of Graham and Powell (1984) were applied to 6/2. For garnet core–phengite core pairs in 6/2, the garnet–phengite geothermometers of Krogh and

Raheim (1978) and Green and Hellman (1982) yielded temperatures of 441–454 °C and 449–460 °C (at 12 kbar), respectively (Table 10). The garnet–amphibole calibration of Graham and Powell (1984) gives consistent temperatures of 444–462 °C and 440–445 °C for garnet core—matrix glaucophane core pairs in sample 6/2 and 106 for blueschist facies metamorphism. For the greenschist facies overprint, temperatures of 409–425 °C were estimated between garnet rim and barroisite overgrowth on matrix glaucophane for sample 6/2 (at 7 kbar). Chlorite Fe/Mg exchange geothermometry of Jowett (1991) for ripidolite derived from glaucophane in sample 6/2 indicates temperatures of 408–412 °C for epidote–amphibole facies overprint.

Chloritoid–phengite schist sample 101 was used for thermodynamic modeling with the aim to *P–T* estimation in the Gündoğmuş Nappe (Fig. 13). The equilibrium field of the assemblage chloritoid + phengite ($Si^{4+} = 3.36$–3.42 p.f.u) + zoisite + chlorite ($X_{Mg} = 0.16$–0.18) + albite + quartz indicate 435–480 °C and 11–13 kbar for blueschist facies metamorphism. Chloritoid X_{Mg} isopleths (0.04–0.06) coincide with the equilibrium boundaries of the assemblage. White mica isopleths for lower Si^{4+} contents (3.20–3.24 p.f.u.) intersect in the equilibrium field at 375–460 °C/6–7 kbar. Although similar pressure estimates for the retrograde Barrovian overprint have been obtained for Alanya and Gündoğmuş areas, temperature seem to have been > 60–70 °C higher in Alanya area, which is consistent with the presence of garnet and biotite in the higher grade domain (Kargıcak Nappe) (Fig. 1b).

P–T estimation for Gündoğmuş area point to blueschist facies imprint at 435–480 °C/11–13 kbar and subsequent retrogression of at epidote–amphibolite facies to greenschist facies conditions of 375–460 °C/6–7 kbar (Fig. 12).

Geochronology

Mica $^{40}Ar/^{39}Ar$ geochronology

Sample preparation and analytical technique

^{40}Ar–^{39}Ar white mica geochronology was carried out on five samples of the Alanya area (Sugözü and Kargıcak Nappe) and four samples of the Gündoğmuş area (Gündoğmuş Nappe). From the Alanya area, we extracted, for the Sugözü Nappe, high-Si phengite (Si^{4+}: 3.46–3.53 p.f.u.) from two eclogite facies samples (193/15A; 115/4A), phengite with lower celadonite content (0.11–0.18) from one blueschist facies metapelite sample (54) and muscovite from one metabasic (garnet–amphibolite) sample (28/4), as well as for the Kargıcak Nappe muscovite one metapelite sample (341/5) containing muscovite. From the Gündoğmuş area, we extracted phengite (Si^{4+}: 3.51–3.55

Table 4 Selected microprobe analyses of phengite, paragonite and biotite (sample descriptions are given by Table 1)

Sample	314/2 ph	314/2 ph	29/1 ph	87/5 ph	87/5 ph	21/2 ph	21/2 ph	183/1 ms	181 ms	181 ms	6/2 ph	6/2 ph	101 ph	101 ph	101 ph	101 ph	29/1 pg	29/1 pg	183/1 pg	183/1 bt	183/1 bt	181 bt	181 bt
SiO_2	52.74	53.39	50.71	54.16	54.88	54.98	54.50	47.74	47.57	46.85	52.77	55.45	52.03	53.40	51.29	52.71	53.12	52.54	47.52	36.01	36.85	37.89	38.28
TiO_2	0.65	0.57	0.10	0.46	0.27	0.22	0.23	0.31	0.37	0.27	0.14	0.24	0.33	0.15	0.07	0.12	0.36	0.34	0.04	2.12	1.95	1.76	1.62
Al_2O_3	28.91	28.93	38.50	28.48	27.48	27.27	27.15	29.04	30.65	34.13	27.21	25.15	28.80	29.69	38.54	38.41	28.97	27.63	38.50	18.82	19.23	17.49	18.04
FeO	2.93	2.60	0.80	3.12	3.33	3.27	3.50	3.28	4.00	2.27	5.16	4.24	4.54	3.08	0.79	0.63	2.82	2.52	0.51	17.53	16.03	15.67	15.03
MnO	0.01	0.02	0.00	0.04	0.00	0.00	0.02	0.00	0.01	0.00	0.22	0.01	0.04	0.00	0.01	0.00	0.00	0.04	0.00	0.05	0.04	0.04	0.06
MgO	3.15	3.07	0.16	2.89	2.99	2.99	2.94	2.48	1.61	0.67	2.80	3.77	4.16	2.99	0.24	0.22	2.95	2.75	0.20	10.48	10.67	11.76	11.88
CaO	0.60	0.96	0.21	0.01	0.01	0.39	0.41	0.02	0.02	0.01	0.02	0.23	0.15	0.01	0.19	0.20	0.02	0.00	0.05	0.02	0.04	0.14	0.08
Na_2O	0.03	0.03	4.09	0.74	0.49	0.03	0.01	0.64	0.85	1.31	0.23	0.02	0.46	0.43	3.84	3.61	0.64	0.65	7.26	0.17	0.15	0.21	0.14
K_2O	6.30	6.81	0.73	6.59	6.67	7.52	7.78	9.48	9.59	9.50	7.29	8.56	6.34	7.39	0.86	1.07	5.87	8.15	0.36	9.14	8.88	8.43	8.54
Total	95.31	96.37	95.29	96.49	96.12	96.68	96.53	92.99	94.67	95.01	95.86	97.66	96.85	97.13	95.83	96.96	94.73	94.60	94.44	94.34	93.84	93.39	93.66
Calculated on the basis of 11 oxygens																				*Calc. on the basis of 22 oxy.*			
Si	3.42	3.44	3.18	3.48	3.54	3.54	3.52	3.27	3.22	3.13	3.47	3.57	3.36	3.42	3.20	3.24	3.45	3.47	3.05	6.40	6.49	6.91	6.94
Ti	0.03	0.03	0.00	0.02	0.01	0.01	0.01	0.02	0.02	0.01	0.01	0.01	0.02	0.01	0.00	0.01	0.02	0.02	0.00	0.01	0.01	0.04	0.03
Al	2.21	2.19	2.85	2.16	2.09	2.07	2.07	2.35	2.44	2.69	2.11	1.91	2.19	2.24	2.83	2.79	2.22	2.15	2.92	5.67	5.57	4.44	4.30
Fe	0.16	0.14	0.04	0.17	0.18	0.18	0.19	0.19	0.23	0.13	0.28	0.23	0.25	0.17	0.04	0.03	0.15	0.14	0.03	0.08	0.06	0.31	0.28
Mn	0.00	0.00	0.00	0.00	0.00	0.00	0.00	0.00	0.00	0.00	0.01	0.00	0.00	0.00	0.00	0.00	0.00	0.00	0.00	0.00	0.00	0.00	0.00
Mg	0.30	0.29	0.02	0.28	0.29	0.29	0.28	0.25	0.16	0.07	0.27	0.36	0.40	0.29	0.02	0.02	0.29	0.27	0.02	0.05	0.05	0.57	0.54
Ca	0.04	0.07	0.01	0.00	0.00	0.03	0.03	0.00	0.00	0.00	0.00	0.02	0.01	0.00	0.01	0.01	0.00	0.00	0.00	0.03	0.03	0.00	0.00
Na	0.00	0.00	0.50	0.09	0.06	0.00	0.00	0.09	0.11	0.17	0.03	0.00	0.06	0.05	0.46	0.43	0.08	0.08	0.69	0.90	0.93	0.16	0.17
K	0.52	0.56	0.06	0.55	0.62	0.64	0.64	0.83	0.83	0.81	0.61	0.70	0.52	0.60	0.07	0.08	0.43	0.46	0.03	0.93	0.86	0.97	1.37
Ms	0.99	0.99	0.10	0.90	0.90	0.99	1.00	0.91	0.88	0.83	0.95	1.00	0.90	0.92	0.13	0.16	0.86	0.89	0.03				
Pg	0.01	0.01	0.90	0.10	0.10	0.01	0.00	0.09	0.12	0.17	0.05	0.00	0.10	0.08	0.87	0.84	0.14	0.11	0.97				

ms muscovite, *ph* phengite, *pg* pargonite, *bt* biotite, Fe^{3+} was estimated by charge balance

Table 5 Selected microprobe analyses of chlorite (sample descriptions are given by Table 1)

Sample	181	181	183/1	183/1	106	106	30	21/2
SiO_2	25.44	26.76	25.27	25.40	26.38	29.59	25.58	23.02
TiO_2	0.06	0.10	0.12	0.12	0.06	0.05	0.10	0.05
Al_2O_3	22.37	22.90	22.04	22.15	19.99	18.48	22.21	36.06
FeO	21.46	20.45	22.25	22.63	27.16	26.68	21.49	24.18
MnO	0.14	0.11	0.05	0.06	0.06	0.07	0.14	0.15
MgO	17.44	16.10	16.63	16.43	15.22	14.38	17.33	2.82
CaO	0.04	0.13	0.00	0.01	0.03	0.10	0.02	0.03
Na_2O	0.01	0.03	0.00	0.00	0.04	0.24	0.00	0.02
K_2O	0.06	0.94	0.01	0.02	0.01	0.09	0.01	0.00
F	0.00	0.00	0.00	0.00	0.00	0.00	0.00	0.05
Total	87.01	87.51	86.38	86.81	88.93	89.68	86.88	86.36
Cations per 14 oxygens								
Si	2.64	2.75	2.66	2.66	2.76	3.04	2.66	2.40
Ti	0.00	0.01	0.01	0.01	0.00	0.00	0.01	0.00
Al	2.74	2.78	2.73	2.74	2.47	2.24	2.72	4.43
Fe	1.87	1.76	1.96	1.98	2.38	2.29	1.87	2.11
Mn	0.01	0.01	0.00	0.00	0.00	0.01	0.01	0.01
Mg	2.70	2.47	2.61	2.56	2.37	2.20	2.69	0.44
Ca	0.00	0.01	0.00	0.00	0.00	0.01	0.00	0.00
Na	0.00	0.01	0.00	0.00	0.01	0.05	0.00	0.00
K	0.01	0.12	0.00	0.00	0.00	0.01	0.00	0.00
F	0.00	0.00	0.00	0.00	0.00	0.00	0.00	0.05
Total	9.99	9.92	9.97	9.96	10.00	9.86	9.97	9.39
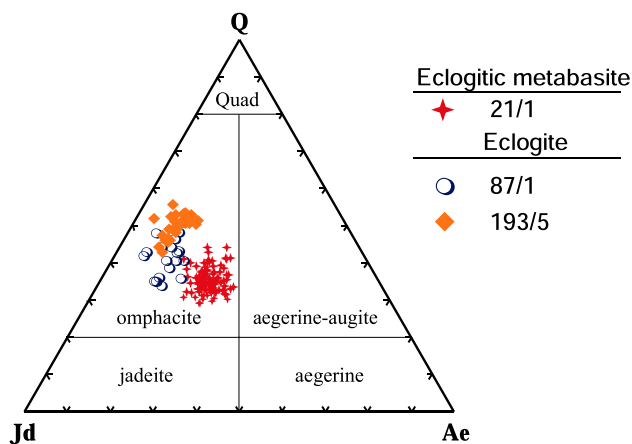
Fig. 8 Plot of clinopyroxenes in a triangular diagram after Morimoto et al. (1988)

p.f.u.) from three blueschist facies samples (metabasites 39/2 and 31/1; metapelite 30) and muscovite from one amphibolite facies metabasite (102/2). Coordinates and descriptions of the samples are given in Table 1. ^{40}Ar–^{39}Ar geochronology by stepwise heating of white mica separates using a CO_2 laser was performed at the University of Potsdam. Pure white mica separates were obtained by crushing of the rock samples using jaw and disk crushers, followed by conventional techniques for mineral separation, including washing, sieving, adherence to paper and handpicking of individual grains under the binocular microscope. For a detailed description of the ^{40}Ar–^{39}Ar geochronology laboratory and analytical procedure, the reader is referred to Wiederkehr et al. (2009).

Dating results

^{40}Ar–^{39}Ar spectra are presented in the Fig. 14. Details of the Ar isotope analyses and J values are given in the Table S1. Plateau ages were calculated for series of adjacent steps that represent individually more than 5 %, and in all more than 50 % of the total ^{39}Ar release, and contiguously agree within 2-SD error limits as McDougall and Harrison (1999). Most of the Ar isotope analyses yielded well-defined age plateaus that represent 86–97 % of the total ^{39}Ar release.

Alanya area: Samples representing the three metamorphic stages identified in the Sugözü Nappe were investigated. High-Si phengite from the eclogitic metapelite sample 193/15A yielded a well-defined plateau age of 83.9 ± 0.9 Ma calculated for four steps out of eight and representing 92 % of the total ^{39}Ar release (Fig. 14a). A similar plateau age was obtained from a second eclogitic metapelite sample (115/4A): 84.8 ± 0.8 Ma as obtained from seven steps out of eleven that represent 91 % of the

Table 6 Selected micropyrobe analyses of omphacite (sample descriptions are given by Table 1)

Sample	314/2	314/2	314/2	21/1	21/1	21/1	87/1	87/1	87/1
SiO_2	55.89	56.12	55.22	56.03	55.82	54.77	56.14	56.63	56.86
TiO_2	0.08	0.07	0.04	0.09	0.04	0.10	0.09	0.06	0.11
Al_2O_3	11.76	9.68	8.36	10.41	9.46	8.99	9.37	11.39	12.44
FeO	4.09	7.13	8.14	8.75	9.87	10.01	7.34	5.65	6.86
MnO	0.00	0.00	0.02	0.03	0.02	0.05	0.04	0.04	0.06
MgO	7.33	7.18	7.56	5.88	5.53	6.12	7.32	6.95	5.26
CaO	12.06	12.49	13.00	9.92	9.94	10.60	12.45	11.95	9.18
Na_2O	7.90	7.62	7.20	8.90	8.97	8.67	7.46	8.15	9.45
K_2O	0.00	0.00	0.00	0.00	0.01	0.00	0.01	0.01	0.01
Cr_2O_3	0.02	0.02	0.01	0.05	0.01	0.06	0.05	0.02	0.04
Summe	99.13	100.31	99.55	100.05	99.66	99.37	100.27	100.84	100.25
Cations per 6 oxygens									
Si	1.99	2.00	1.99	1.99	2.00	1.97	2.00	1.99	2.01
Al(IV)	0.01	0.00	0.01	0.01	0.00	0.03	0.00	0.01	0.00
Al(VI)	0.48	0.40	0.34	0.43	0.40	0.35	0.39	0.46	0.52
Fe^{2+}	0.05	0.09	0.07	0.07	0.07	0.02	0.10	0.06	0.08
*Fe^{3+}	0.07	0.12	0.17	0.19	0.22	0.28	0.12	0.10	0.13
Mg	0.39	0.38	0.41	0.30	0.30	0.33	0.38	0.36	0.28
Ti	0.00	0.00	0.00	0.00	0.00	0.00	0.00	0.00	0.00
Cr	0.00	0.00	0.00	0.00	0.00	0.00	0.00	0.00	0.00
Na	0.54	0.53	0.50	0.61	0.62	0.60	0.52	0.56	0.65
Ca	0.46	0.48	0.50	0.38	0.38	0.41	0.48	0.45	0.35
Mg	0.00	0.00	0.00	0.01	0.00	0.00	0.01	0.00	0.00
Quad	45	47	49	38	38	39	48	44	35
Jd	48	40	34	43	40	34	40	46	52
Ae	7	13	17	19	22	27	12	10	13

*Fe^{3+} was estimated by charge balance

total ^{39}Ar release (Fig. 14b). Phengite from the blueschist facies metapelite sample, 54 yielded a plateau age of 81.7 ± 0.9 Ma (4 of 9 steps; 86 % of the total ^{39}Ar release) (Fig. 14c). For the amphibolitic metapelite sample 28/4, muscovite gave a plateau age of 78.4 ± 0.7 Ma (6 of 11 steps; 90 % of the total ^{39}Ar) (Fig. 14d). From the Barrovian facies Kargıcak Nappe, muscovite from the metapelite sample 341/5 yielded plateau age of 75.09 ± 2.23 Ma (Fig. 14e).

Gündoğmuş area Phengite from three blueschist facies samples from the Gündoğmuş area yielded the following plateau ages: 81.3 ± 1.0 Ma from metabasite 39/2 (four of eight steps; 93 % of the total ^{39}Ar) (Fig. 14f); 82.8 ± 0.8 Ma from metabasite 31/1 (8 of 10 steps; 97 % of the total ^{39}Ar) (Fig. 14g); and 80.8 ± 0.7 Ma from metapelite 30 (6 of 9 steps; 93 % of the total ^{39}Ar) (Fig. 14h). In addition, in the muscovite from the Barrovian facies metapelite sample 102/2, most of the ^{39}Ar (91 %) was released after two heating steps, pointing to an age of 78.4 ± 1.1 Ma (Fig. 14i).

Age interpretation

Ar–Ar geochronology results provide temporal constraints on the successive metamorphic stages of the Sugözü Nappe: (1) Ar–Ar dates for each metamorphic stage are internally consistent within 1-SD error, even for samples from different areas; (2) eclogite facies phengite dates from the Sugözü Nappe are consistently older than those obtained from the retrograde blueschist facies phengites. Muscovite from the Mahmutlar garnet–mica schist yielded in turn younger dates than any of those from HP–LT samples. In addition, all Ar–Ar dates for the blueschist facies in the Gündoğmuş area overlap within 1-SD error and are identical to that for the retrograde blueschist facies in the Alanya area.

On the basis of Ar/Ar dating results, we thus infer that in the Sugözü Nappe eclogitic paragenesis formed around 84 Ma and were then overprinted in the blueschist facies until ca. 80 Ma. Barrovian-type metamorphism witnessing transition to a continental-collision stage followed up around 78–75 Ma. Similarly for Gündoğmuş area,

Table 7 Selected microprobe analyses of epidote/clinozoisite (sample descriptions are given by Table 1)

Sample	87/1	87/1	79/2	79/2	193/5	198/1B	198/1B	101	101
SiO_2	37.94	37.82	38.31	39.23	37.91	38.83	39.14	37.83	37.74
TiO_2	0.23	0.05	0.12	0.18	0.08	0.21	0.19	0.02	0.00
Al_2O_3	23.10	22.54	24.85	25.78	23.07	26.38	26.59	24.84	25.07
Fe_2O_3	10.84	12.29	6.95	5.92	11.16	6.99	6.67	11.88	11.80
MnO	0.37	0.18	0.03	0.02	0.18	0.04	0.00	0.13	0.08
MgO	0.05	0.03	0.03	0.07	0.00	0.07	0.06	0.02	0.01
CaO	22.97	23.51	23.85	24.05	23.78	23.62	23.73	23.51	23.60
Na_2O	0.03	0.05	0.00	0.00	0.00	0.01	0.02	0.02	0.00
K_2O	0.01	0.00	0.00	0.01	0.01	0.01	0.01	0.00	0.01
Cr_2O_3	0.03	0.00	0.02	0.01	0.03	0.04	0.01	0.00	0.00
Total	95.57	96.47	94.16	95.27	96.21	96.19	96.41	98.24	98.30
Cations per 12.5 oxygens									
Si^{4+}	3.07	3.05	3.10	3.12	3.06	3.07	3.08	2.99	2.98
Ti^{4+}	0.01	0.00	0.01	0.01	0.00	0.01	0.01	0.00	0.00
Al_{3+}	2.21	2.15	2.37	2.42	2.19	2.46	2.47	2.31	2.33
Fe^{3+}	0.66	0.75	0.42	0.35	0.68	0.42	0.40	0.71	0.70
Mn^{2+}	0.03	0.01	0.00	0.00	0.01	0.00	0.00	0.01	0.01
Mg^{2+}	0.01	0.00	0.00	0.01	0.00	0.01	0.01	0.00	0.00
Ca^{2+}	1.99	2.03	2.07	2.05	2.05	2.00	2.00	1.99	1.99
Na^{1+}	0.01	0.01	0.00	0.00	0.00	0.00	0.00	0.00	0.00
K^{1+}	0.00	0.00	0.00	0.00	0.00	0.00	0.00	0.00	0.00
Cr^{3+}	0.00	0.00	0.00	0.00	0.00	0.00	0.00	0.00	0.00
Total	7.98	8.00	7.99	7.98	8.00	7.98	7.97	8.01	8.01

Fe^{3+} was estimated by charge balance

blueschist facies metamorphism and following Barrovian overprint were dated at 80–82 and 78 Ma, respectively.

Zircon U/Pb geochronology

Sample preparation and analytical technique

Whole rock powder was obtained by crushing and splitting from about 30-kg rock samples. The selected representative zircons were separated at the Department of Geology Engineering, Dokuz Eylül University, Turkey. Zircons from two eclogite samples (193/2A and 198/1B) were extracted using standard procedures such as Wilfley table, magnetic separator and heavy liquids. They were hand-picked under a binocular microscope and then were finally embedded in epoxy resin for analysis. The mounts were polished down to approximately one-third of thickness and were taken transmitted- and reflected-light images to document cracks and inclusions in zircons. The internal structures of zircons were documented by cathodoluminescence (CL) using a CAMECA SX51 instrument at conditions of 15 kV and 120 nA in Institute of Geology and Geophysics, Chinese Academy of Sciences, Beijing (IGG-CAS). Coordinates and descriptions of the samples are given in Table 1.

Zircon U–Pb dating of samples 193/2A and 198/1B were performed using Laser Ablation Inductively Coupled Plasma Mass Spectrometry (LA-ICP-MS) at University of Science and Technology of China in Hefei. A pulsed 193 nm ArF Excimer laser system with 10 J/cm² beam energy at a repetition ratio of 10 Hz coupled to a PerkinElmer Elan DRCII quadrupole ICP-MS was used for ablation. Spot size generally was 60 μm in diameter, sometimes 44 μm where necessary. Common Pb correction was applied using the method of Andersen (2002). Uncertainties of individual analyses are reported at 1ó; weighted average ages are calculated at 2ó level and uncertainties in ages are reported at the 95 % confidence level. For detailed analytical procedure see Yuan et al. (2004). Standard zircon 91500 was analyzed to calibrate the mass discrimination and elemental fractionation, the U/Pb ratios were processed using a macro program LaDating@Zrn written in Excel spreadsheet software. The age calculations and concordia diagrams were obtained using Isoplot/ Ex (ver. 3.75) program o Ludwig (2012).

Sample 193/2A Zircons from this sample are clear, often transparent and with euhedral to subhedral crystal shapes. They are 70–150 μm in size with aspect ratios range from stubby (1:1) to elongated (1:3). Most grains display oscilla-

Table 8 Selected microprobe analyses of plagioclase (sample descriptions are given by Table 1)

Sample	6/2	101	183/1	181	54	54	193/15	193/15	341/5	341/5
SiO_2	73.23	72.85	61.82	61.75	70.94	68.28	69.83	69.95	67.71	68.79
TiO_2	0.02	0.03	0.00	0.00	0.02	0.02	0.03	0.02	0.03	0.01
Al_2O_3	20.46	19.82	23.33	23.46	19.74	18.70	18.61	18.68	21.11	20.96
FeO	0.16	0.29	0.12	0.14	0.02	0.04	0.02	0.02	0.19	0.05
MnO	0.02	0.01	0.00	0.00	0.01	0.00	0.00	0.03	0.00	0.02
MgO	0.01	0.00	0.00	0.00	0.01	0.00	0.00	0.00	0.00	0.00
CaO	0.25	0.32	5.26	5.43	0.70	0.70	0.17	0.12	2.97	2.82
Na_2O	5.00	6.89	8.52	8.55	10.32	6.81	11.73	11.66	9.72	9.77
K_2O	0.02	0.05	0.07	0.06	0.13	0.13	0.03	0.05	0.35	0.34
Cr_2O_3	0.00	0.00	0.00	0.00	0.00	0.03	0.02	0.01	0.02	0.00
Total	100.07	99.91	99.12	99.39	101.87	94.72	100.44	100.53	102.10	102.75
Cations per 32 oxygens										
Si^{4+}	13.62	13.22	11.07	11.03	12.32	13.07	12.17	12.18	11.75	11.87
Ti^{4+}	0.00	0.00	0.00	0.00	0.00	0.00	0.00	0.00	0.00	0.00
Al^{3+}	3.37	3.18	3.69	3.70	3.03	3.16	2.87	2.88	3.24	3.20
Fe^{2+}	0.01	0.02	0.01	0.01	0.00	0.00	0.00	0.00	0.01	0.00
Mn^{2+}	0.00	0.00	0.00	0.00	0.00	0.00	0.00	0.00	0.00	0.00
Mg^{2+}	0.00	0.00	0.00	0.00	0.00	0.00	0.00	0.00	0.00	0.00
Ca^{2+}	0.02	0.03	0.51	0.52	0.06	0.07	0.02	0.01	0.28	0.26
Na^{1+}	0.45	0.61	0.74	0.74	0.87	0.63	0.99	0.98	0.82	0.82
K^{1+}	0.00	0.00	0.00	0.00	0.01	0.01	0.00	0.00	0.02	0.02
Cr^{3+}	0.00	0.00	0.00	0.00	0.00	0.00	0.00	0.00	0.00	0.00
Total	17.48	17.06	16.02	16.01	16.29	16.95	16.05	16.07	16.12	16.16
% An	0.05	0.05	0.25	0.26	0.07	0.10	0.02	0.01	0.25	0.24

Fe^{3+} was estimated by charge balance

tory growth zoning with narrow or moderate bands which are consistent with a primary magmatic origin and dominantly narrow rims (<20 microns) of high luminosity (Fig. 15). Zircon analyses from the oscillatory zoned domains have Th and U contents ranging from 112 to 617 and 318 to 1,077 ppm, respectively. Their Th/U ratios are between 0.2 and 0.9. A total of 18 spots were analyzed on 16 grains. Only the data with a concordant percentage $[(^{206}Pb/^{238}U)/(^{207}Pb/^{235}U)*100]$ between 95 % and 105 % are chosen for calculation. Majority of the ages obtained are clustered between 619 Ma and 641 Ma, with the exception of two grains that represent anomalously older ages (gr 1c: 669 ± 12 and gr 3: 675 ± 12 Ma). Excluding these anomalous ages, the concordia age calculated from eight concordant zircon population is 629.0 ± 2.6 Ma (n = 8, MSWD = 0.01) (Table S2; Fig. 16a, b). Similarly, they yield a weighted mean age of 629.4 ± 8.1 Ma (95 % confidence, MSWD = 0.56) and TuffZirc Age of 630.5 + 8.5–11.5 Ma. Therefore, we interpret that the concordia age of 629 ± 3 Ma reflects the time of crystallization of magmatic protolith of eclogite. Four inherited grains and three discordant rims yielded ages between 562 and 1,858 Ma and between 749 and 2,884 Ma, respectively. Because the rims with high luminosity are very narrow, the age of HP metamorphism was not determined in this sample.

Sample 198/1B Zircons from this sample are clear, often transparent and with euhedral to subhedral crystal shapes. They are 100–250 µm in size with aspect ratios range from stubby (1:1) to elongated (1:4). CL imaging illustrates the complexity of zircon crystallization of this sample with inherited cores consisting of fragments or whole, rounded grains surrounded by bright luminescent rims. Some cores have angular and fractured shape with no zoning, oscillatory zoning and planar zoning. Almost, all zircon grains are surrounded by unzoned or ghost-oscillatory zoned, bright luminescent rims representing HP metamorphism (Fig. 15). Thirty-one spots from cores and twenty-eight spots from rims were analyzed on 48 grains. Only the data with a concordant percentage $[(^{206}Pb/^{238}U)/(^{207}Pb/^{235}U)*100]$ between 95 and 105 % are chosen for calculation. Zircon analyses from the oscillatory zoned domains have Th and U contents ranging from 64 to 627 and 196 to 1,491 ppm, respectively. Their Th/U ratios are between 0.1 and 1.1. Sixteen concordant analyses from zircon cores yielded a wide range of ages between 621 Ma and 2,155 Ma. The fewer amounts of concordant analyses indicate that the sample was affected by both recent and ancient Pb-loss trajectories. For this reason, the age of protolith of this sample was not determined. The age data indicate the existence of a number of inherited grains in this sample. Zircon analyses from rims

Table 9 Selected microprobe analyses of chloritoid (sample descriptions are given by Table 1)

Sample	101	101	101	101	101	101
SiO_2	24.09	23.84	23.99	24.07	24.03	23.78
TiO_2	0.05	0.01	0.07	0.01	0.08	0.03
Al_2O_3	40.14	39.38	39.81	39.21	39.00	38.78
FeO	26.25	27.17	26.09	26.26	26.95	27.48
MnO	0.14	0.12	0.24	0.62	0.59	0.57
MgO	1.64	1.63	2.07	2.05	1.57	1.38
CaO	0.01	0.01	0.02	0.01	0.01	0.00
Na_2O	0.00	0.01	0.01	0.01	0.00	0.00
K_2O	0.02	0.00	0.01	0.00	0.00	0.00
Total	92.33	92.17	92.30	92.22	92.22	92.02
Structural formula based on 4 (Si, Al) and 6 (Al, Fe, Mn, Mg)						
Si	2.012	1.996	1.998	2.013	2.021	2.004
Ti	0.003	0.001	0.004	0.000	0.005	0.002
Al	3.952	3.886	3.909	3.865	3.866	3.851
Fe^{3+}	0.048	0.114	0.091	0.135	0.134	0.149
Fe^{2+}	1.786	1.789	1.727	1.702	1.762	1.787
Mn	0.010	0.008	0.017	0.044	0.042	0.040
Mg	0.102	0.101	0.128	0.127	0.098	0.086
Ca	0.001	0.001	0.002	0.001	0.001	0.000
Na	0.001	0.001	0.001	0.001	0.000	0.000
K	0.002	0.000	0.001	0.000	0.000	0.000
Al VI	1.985	2.003	1.997	1.986	1.974	1.995
Al IV	1.968	1.883	1.911	1.879	1.892	1.856
X_{Mg}	0.05	0.05	0.07	0.06	0.05	0.04

Fe^{3+} was estimated by charge balance

have Th and U contents ranging from 0.2 to 216 and 8 to 229 ppm, respectively, and their Th/U ratios are between 0.01 and 0.9. The ages of twelve concordant analyses from rims range from 77 to 2,051 Ma. Clustered six of them give a concordia age of 84.7 ± 1.5 Ma ($n = 6$, MSWD = 1.4) (Table S2; Fig. 16c, d). They yield a weighted mean age of 84.0 ± 4.8 Ma (95 % confidence, MSWD = 0.38) and TuffZirc Age of 83.5 + 5.5–6.5 Ma. We interpret that the concordia age of 84.7 ± 1.5 Ma reflects the time of eclogite facies metamorphism in Sugözü nappe.

Rutile U/Pb geochronology

Sample preparation and analytical technique

Thin section of sample 5/9 for U–Pb rutile analyses was polished to about 50 μm in thickness. U–Pb dating of rutile was conducted at the Department of Earth Sciences at the University of Gothenburg using New Wave NWR 213 laser ablation system coupled to an Agilent 8800QQQ quadropole ICP-MS. Rutiles were measured in situ from thin section. The sample was ablated in spots of 50 μm at a laser fluence of 5.6 J/cm2 and a repetition rate of 5 Hz. Signals were recorded for 60 s per spot after measuring a gas blank of 20 s for background subtraction before each spot. A He–Ar mixture was used as carrier gas (0.70 l/min). Helium gas, which carries the laser ablated sample aerosol from the sample cell, is mixed with argon carrier gas and nitrogen as additional diatomic gas to enhance sensitivity, and, finally, flows into the ICPMS torch. The U–Pb ratio and elemental concentrations were standardized against R10 (ca. 30 ppm, 1,095 Ma, Luvizotto and Zack 2009).

Sample 5/9 The U–Pb analyses of rutile standard R10 from south Norway (Luvizotto and Zack 2009) used in this study are given in Table S3 and Fig. 17a. The U–Pb data of rutiles in 5/9 are also shown in Table S3 and Fig. 17b. For standard R10, the $^{206}Pb/^{238}U$ ages are consistent within 1.1 % (1σ) (Fig. 17a). The $^{207}Pb/^{206}Pb$ ratios are indiscernible within errors and yield average of 0.07580 ± 0.0009. R10 was dated at 1,091 ± 11 Ma, which is well identical to TIMS result of 1,090 ± 5 Ma (Luvizotto and Zack 2009).

In eclogitic metabasite sample 5/9, ten spot analyses were performed on six rutile crystals with diameter of 50 μm. The U contents range between 3 ppm and 5 ppm (Table S3). On the Terra–Wasserburg plot, linear regression of the data point (MSWD = 1.2) gives a lower intercept age of 82 ± 3 Ma and the upper intercept with

Table 10 Conventional geothermometry estimation results

Sample no	Pairs	grt–ph ther.		grn–amp ther.	grt–cpx thermometry						grt–bt ther.			Zr in rutile			
		*1	*2	*3	*4	*5	*6	*7	*8	*9	*10	*11	*12	*13	*14	*15	*16
21/1	grt–amp(inc)			450–508													
21/1	grt(r)–cpx				556–576	537–567	523–554	467–488	455–481	513–553							
314/2	grt(c)–amp(inc)			457–488													
314/2	grt(r)–amp			503–509													
314/2	grt(r)–cpx				516–556	502–534	504–542	440–478	426–474	498–519							
87/1	grt(r)–cpx				549–572	529–551	515–525	473–498	462–497	514–522							
29/1	grt(c)–amp(c)			397–421													
29/1	grt(r)–amp(c)			483–533													
87/5	grt–ph		515–555														
21/2	grt–ph(inc)		521–557														
181	grt(r)–bt(r)										442–456	451–465	457–479				
183/1	grt(r)–bt(r)										443–459	447–471	461–485				
181	grt(r)–ms(r)		538–551														
183/1	grt(r)–ms(r)		542–561														
6/2	grt(c)–ph(c)	441–454	444–462														
6/2	grt(r)–amp(r)		409–425														
106	grt(c)–ph(c)	449–460	440–445														
5/9	Rutile													587	565	567	616

*1: Krogh and Raheim (1978); *2: Green and Hellman (1982); *3: Graham and Powell (1984); *4: Ellis and Green (1979); *5: Powell (1985); *6: Krogh (1988); *7: Ai (1994); *8: Krogh Ravna (2000); *9: Nakamura (2009); *10: Thompson (1976); *11: Hodges and Spear (1982); *12: Perchuck and Lavrenteva (1983); *13: Zack et al.(2004); *14: Watson et al. (2006); *15: Ferry and Watson (2007); *16: Tomkins et al. (2007)

grt garnet, amp amphibole, cpx clinopyroxene, ph phengite, bt biotite, ms muscovite, c core, r rim, ther thermometry
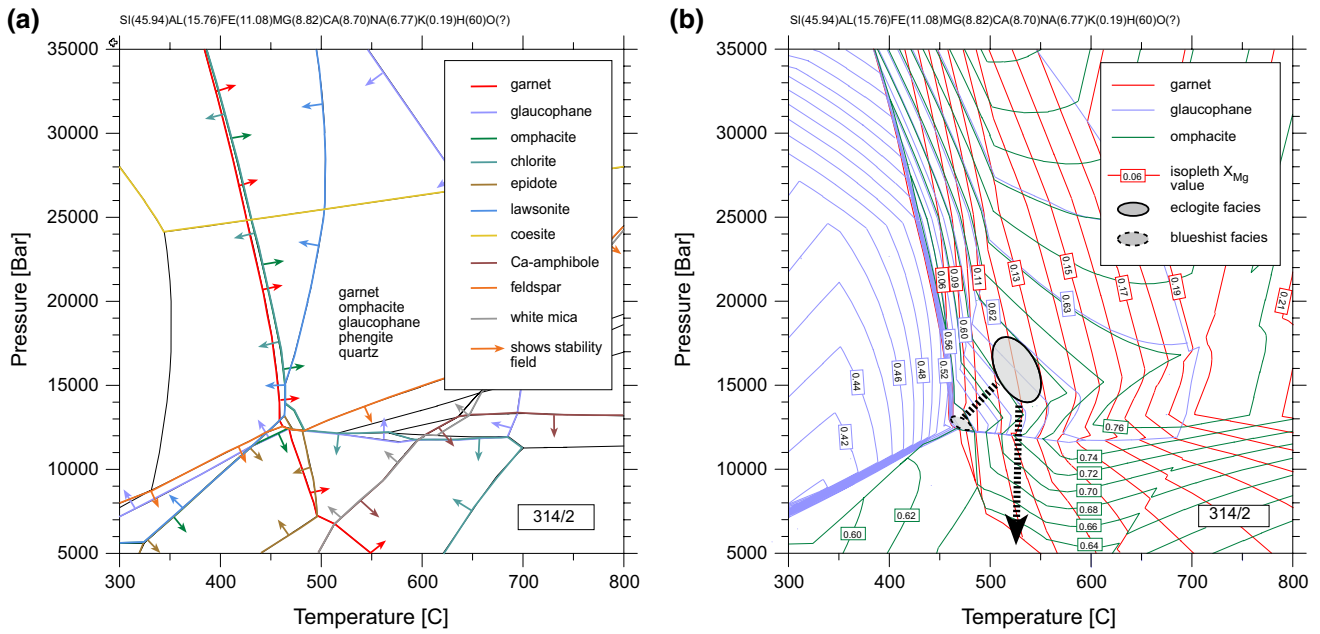
Fig. 9 The equilibrium phase diagram for sample 314/2 (eclogitic metabasite), calculated by the means of THERIAK-DOMINO software (de Capitani and Brown 1987). Bulk chemistry of the sample is shown as normalized major element content. **a** The *colored arrows* depict the stability domain of the major phases in the rock, **b** compositional X_{Mg} contours
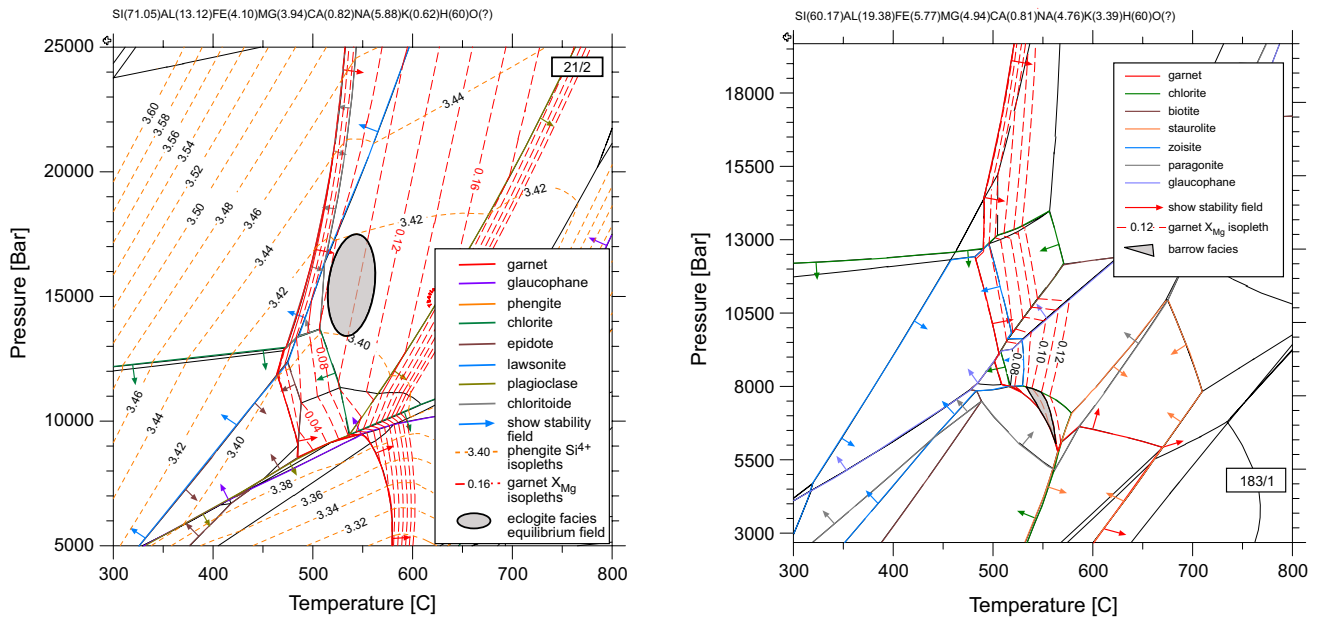
Fig. 10 The equilibrium phase diagram for sample 21/2 (garnet–glaucophane–phengite schist), calculated by the means of THERIAK-DOMINO software (de Capitani and Brown 1987). Bulk chemistry of the sample is shown as normalized major element content

Fig. 11 The equilibrium phase diagram for sample 183/1 (garnet–biotite–chlorite schist), calculated by the means of THERIAK-DOMINO software (de Capitani and Brown 1987). Bulk chemistry of the sample is shown as normalized major element content

$^{207}Pb/^{206}Pb = 0.0032 \pm 0.0016$ for the common Pb composition (Fig. 17b).

Rutile U–Pb ages tend to exhibit younger U–Pb ages than the coexisting titanite and zircon U–Pb ages and even hornblende $^{40}Ar/^{39}Ar$ ages (Mezger et al. 1991;

Corfu and Easton 1995; Li et al. 2003, 2011; Zack et al. 2011). This can be attributed to radiogenic Pb diffusion in rutile and thus to the low closure temperature of U–Pb radiometric system in rutile (Gao et al. 2014). Closure
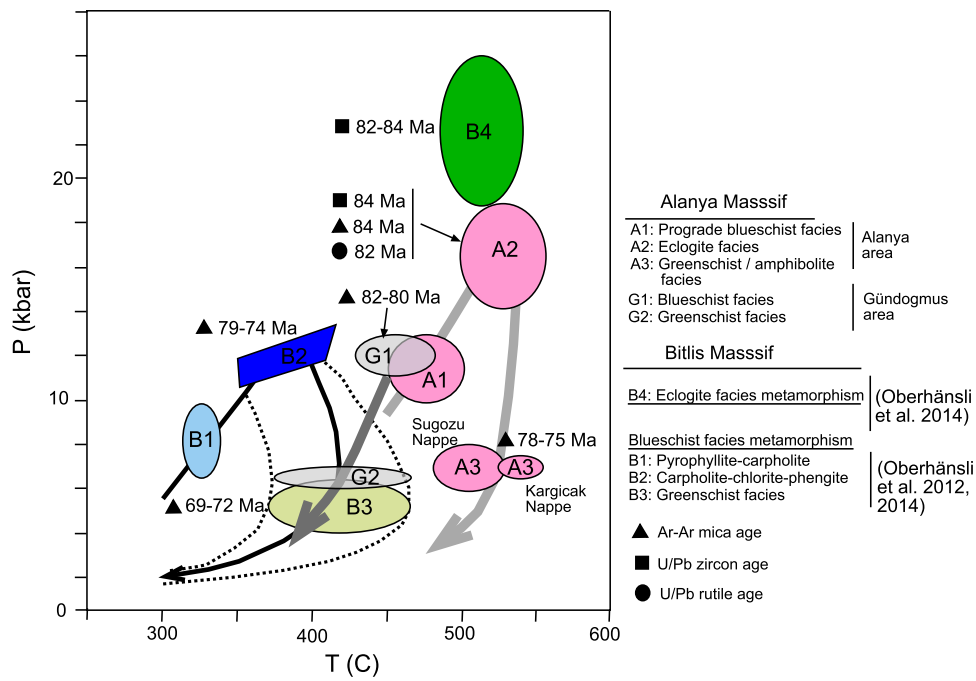
Fig. 12 *P–T* path of Alanya and Gündoğmuş areas and comparison with Bitlis Massif
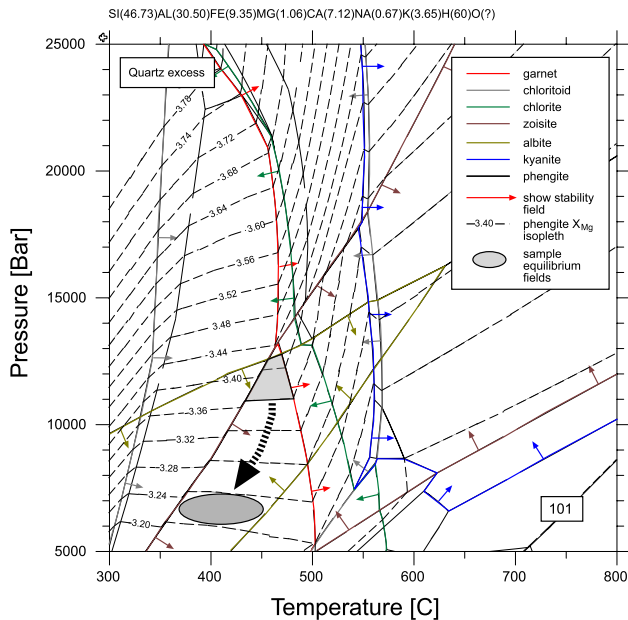
Fig. 13 The equilibrium phase diagram for sample 101 (chloritoid–phengite schist), calculated by the means of THERIAK-DOMINO software (de Capitani and Brown 1987). Bulk chemistry of the sample is shown as normalized major element content

temperature depends on grain size and cooling rate (Cherniak 2000). The U–Pb Tc for rutile is probably between 490 and 640 °C, average 570 °C (Kooijman et al. 2010). The size of rutile grains from sample 5/9 ranges from 50 to ~150 μm. The peak metamorphic conditions of eclogites were estimated as the temperature of 500–567 °C and the pressure of 14–18 kbar. Therefore, the U–Pb rutile age of 82 ± 3 Ma can be interpreted as the time of the eclogite facies metamorphism.

Discussion

Eclogite–blueschist facies metamorphism with epidote–amphibolite overprint in Sugözü and Gündoğmuş nappes and Barrovian-type greenschist facies metamorphism in the other nappe units of the Alanya Massif were dated by both U–Pb zircon and rutile and Ar/Ar white mica methods. U–Pb zircon and rutile dating yield 84 Ma and 82 Ma, respectively, Santonian–Campanian, for eclogite facies metamorphism. Phengitic white micas from the host rock of eclogites give identical ages of about 84 Ma, Santonian. Similar ages of about 80–82 Ma, Campanian, for the blueschist metamorphism are obtained from the eclogite-free Gündoğmuş area. Comparing blueschist (460–480 °C/12–13 kbar-Sugözü nappe) metamorphism and the peak *P/T* conditions of the eclogite (550–567 °C/14–18 kbar) for the Alanya Massif and the closure temperature of white mica (550–600 °C, Villa 1998; Di Vincenzo et al. 2003), these ages may be close to the crystallization age during the eclogite and blueschist facies metamorphism. Furthermore, the white micas with low-Si^{+4} content from Sugözü nappe
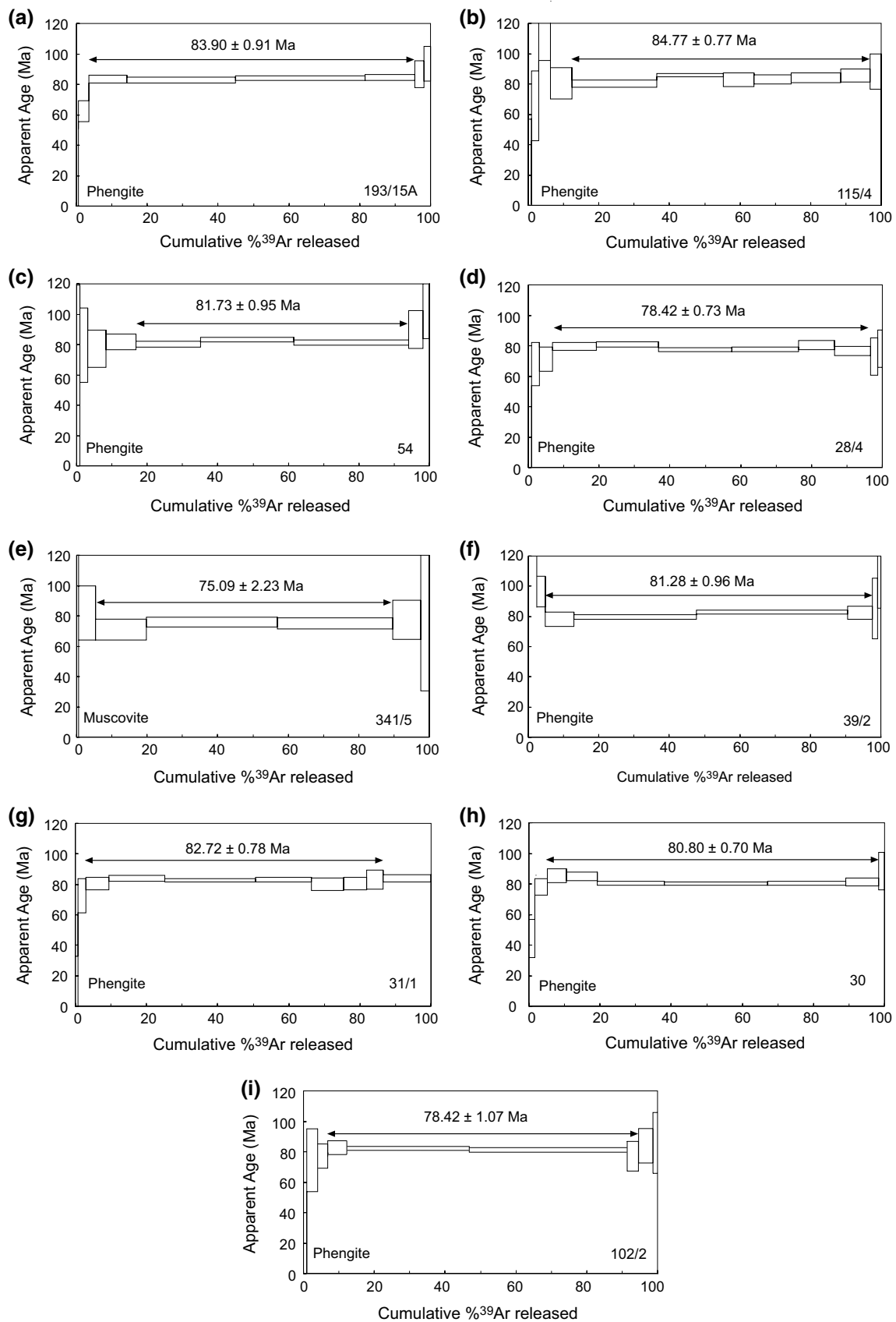
Fig. 14 ^{40}Ar–^{39}Ar spectra of dating samples
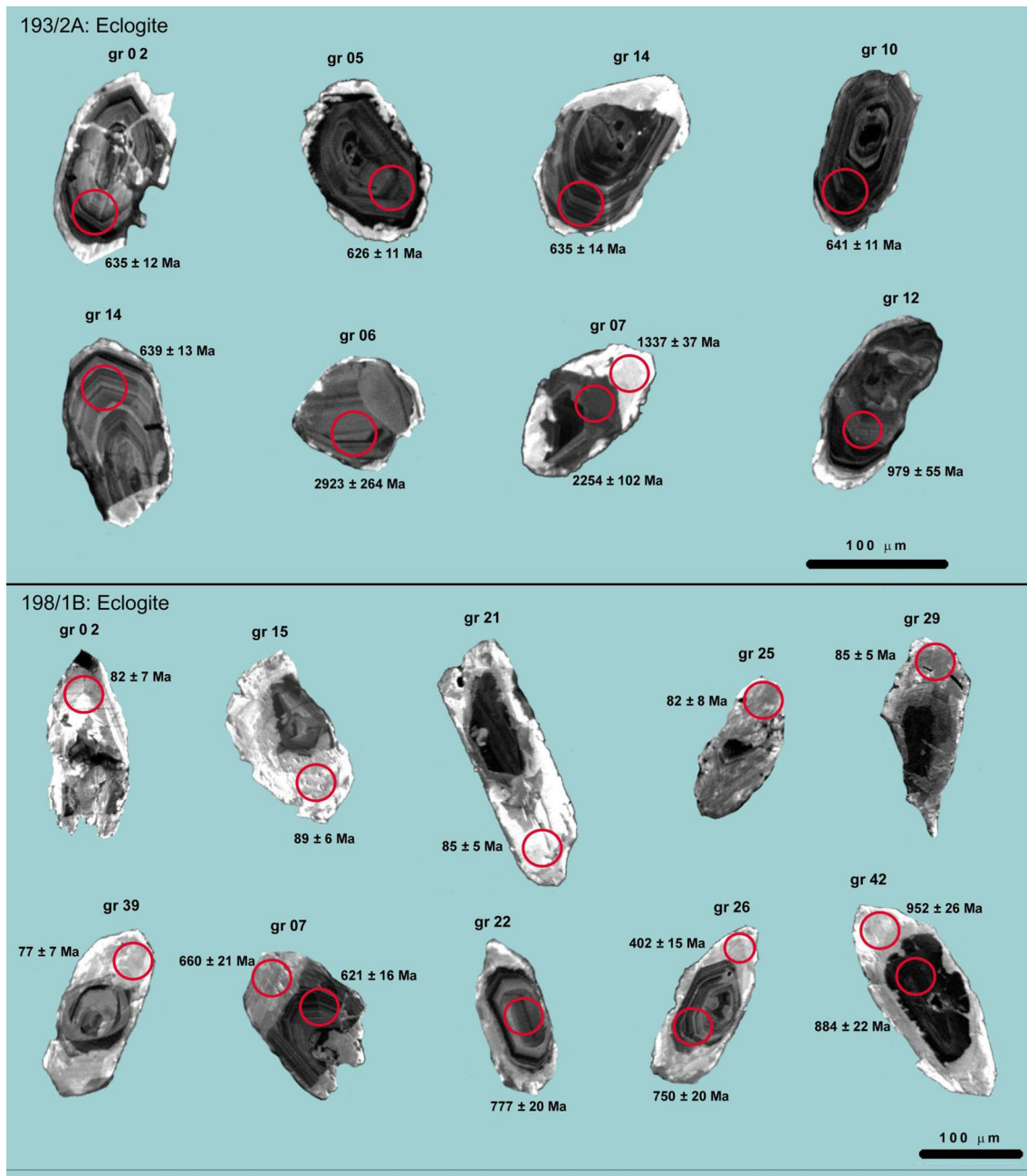
Fig. 15 CL images of selected zircons in sample 193/2A and 198/1B showing LA-ICP-MS analysis spots (*circles*) and $^{206}Pb/^{238}U$ ages

and Gündoğmuş nappe yield ages of about 78 Ma, Campanian, which represents the retrograde overprint of HP assambleges under epidote–amphibolite and greenschist facies conditions.

Spatial and temporal relationship between Alanya HP metamorphism and Cretaceous HP belts of Turkey

As it has been outlined previously, Turkey is made up of several continental blocks, which are separated by suture

zones (Fig. 18). These sutures are believed to be involved in the Late Cretaceous closure history of branches of the Neotethys Ocean. They can be recognized either by accretionary complexes and associated ophiolitic bodies or HP metamorphism, eclogites and/or blueschists. The existence of Pan-African eclogites (530 Ma) in the Menderes Massif (Candan et al. 2001; Oberhänsli et al. 2012), Late Triassic eclogites (203–215 Ma) and blueschist in the Sakarya Zone (Okay and Monié 1997; Okay et al. 2002) and Eocene eclogites and blueschist (ca. 40 Ma) in both the Turkish
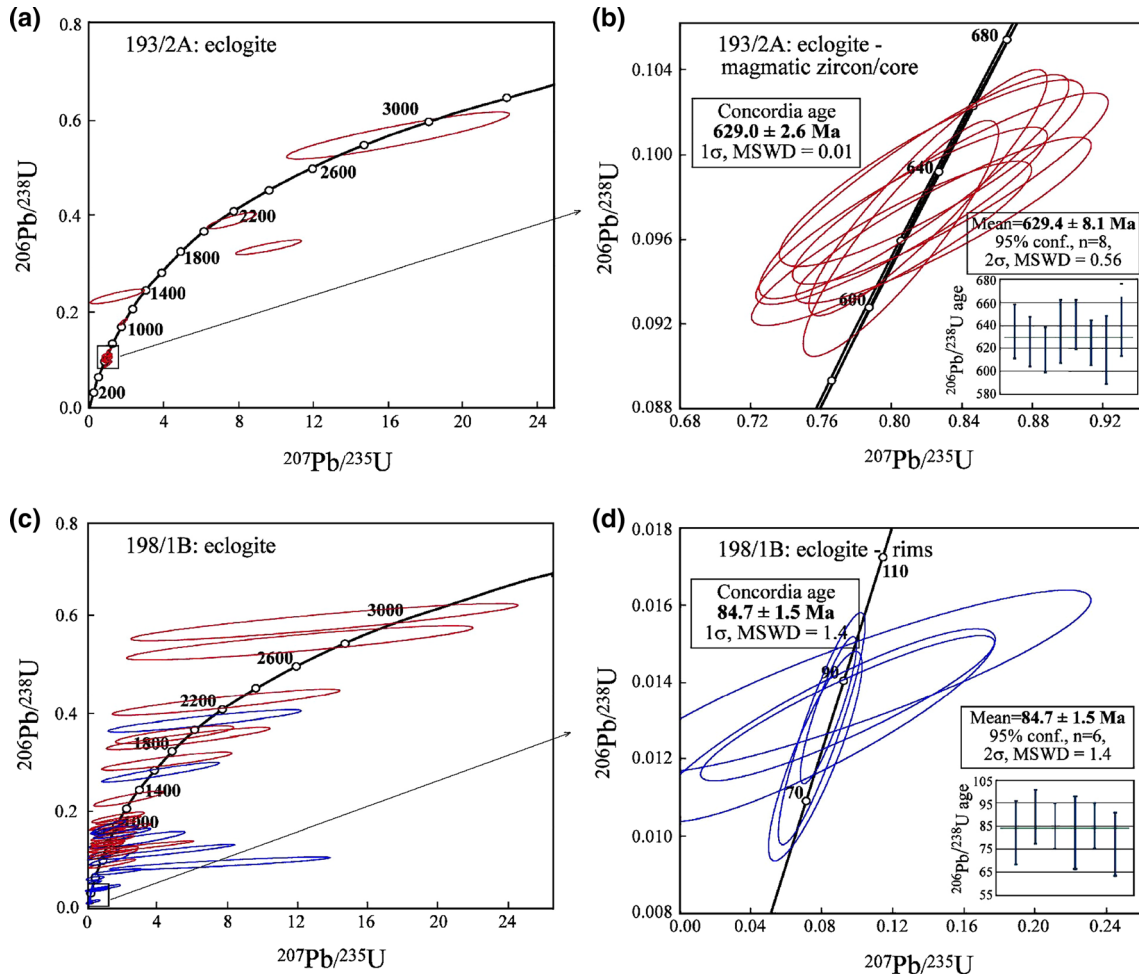
Fig. 16 Concordia diagrams showing U–Pb isotope ratios and ages derived from LA-ICP-MS analyses for eclogite samples 193/2A (**a**, **b**) and 198/1B (**c**, **d**)
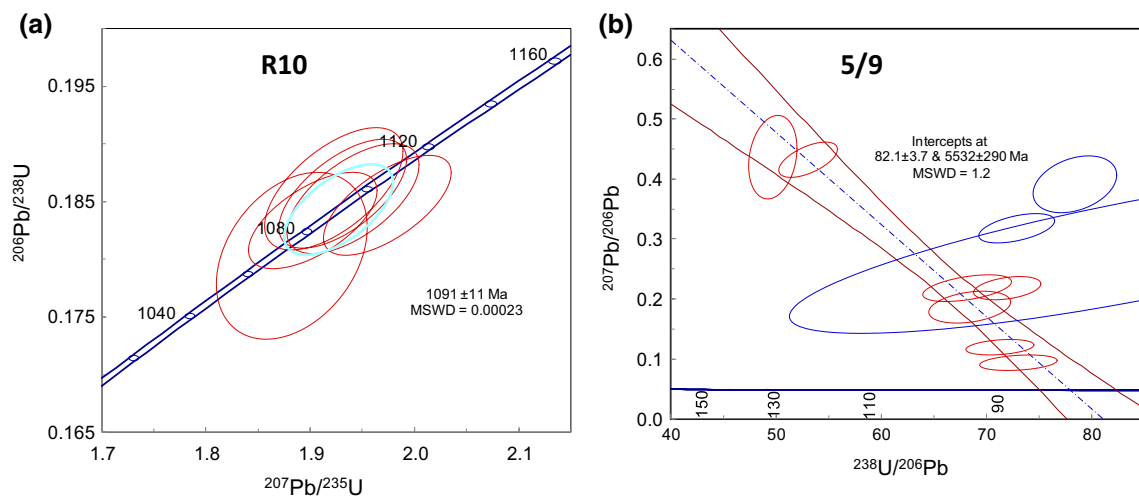
Fig. 17 a U–Pb concordia dagram forrutile used as standard in this study, **b** U–Pb Tera–Wasserburg diagram for rutile from eclogitic metabasite sample 5/9
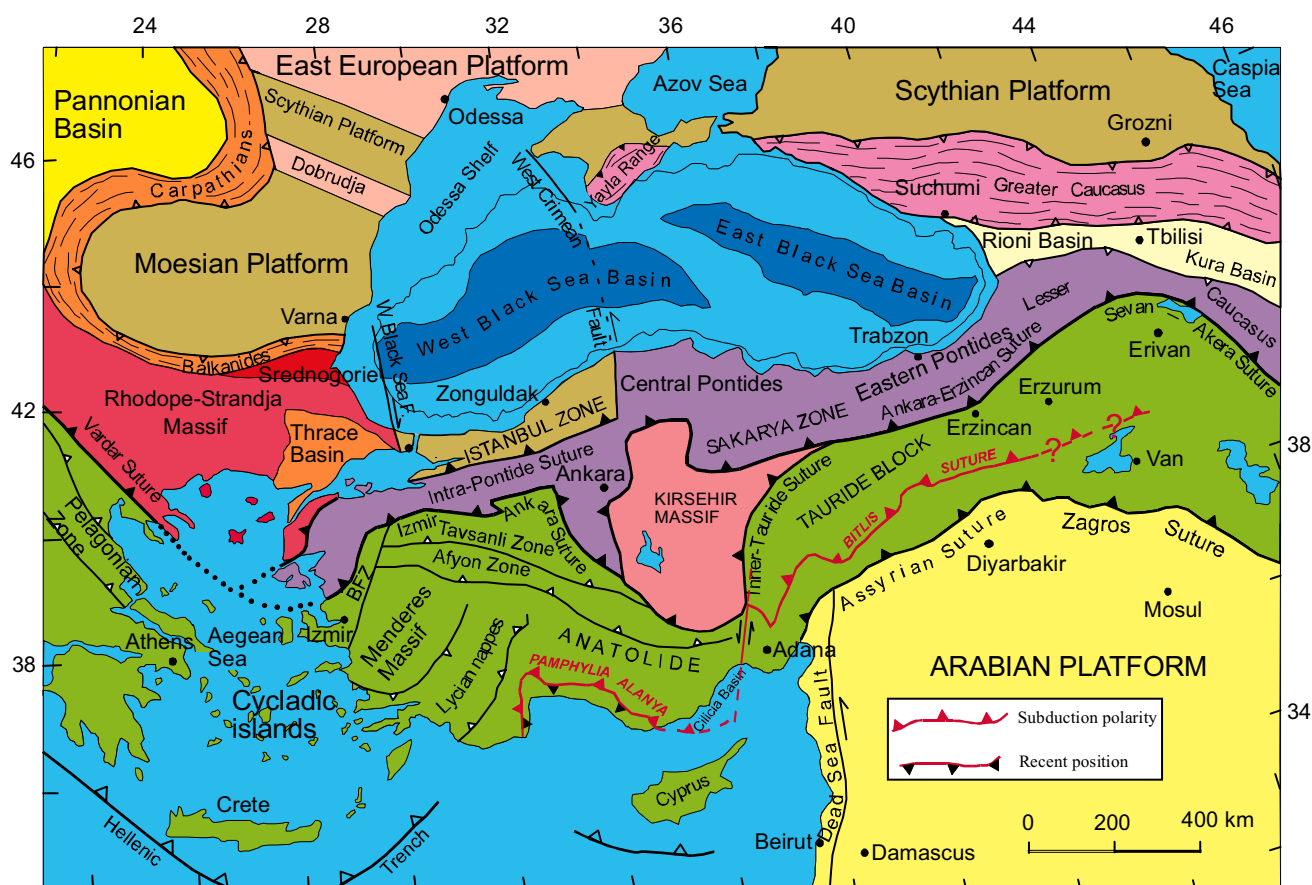
Fig. 18 Main tectonic units and suture zones of Turkey (after Okay and Tüysüz 1999) and location of Pamphylia–Alanya–Bitlis Suture

part of the Cycladic Complex (Candan et al. 1997; Oberhänsli et al. 1998) and in Mesozoic cover of the Menderes Massif (Pourteau et al. 2012) have been documented. However, the great majority of HP rocks in Turkey is Mid- to Late Cretaceous in age.

In the central and western Pontides, Cretaceous HP rocks have been recognized in several localities. In the central Pontides, Kargı Massif, HP rocks, eclogites and associated blueschists are dated at ca. 105 Ma, Albian, by Ar–Ar and Rb–Sr dating methods for white mica. The HP event in this subduction-accretion complex is attributed to a northward subduction of oceanic crust (Okay et al. 2006, 2013). In the western Pontides and Biga Peninsula, HP rocks are more common. An Albian age of about 100 Ma for HP metamorphism was obtained from phengite schist with eclogite lenses occurring as tectonic slices in the Çetmi mélange (Okay and Satır 2000a). In Çamlıca metamorphic rocks, Rb–Sr phengite ages from the pelitic country rocks of the eclogites, occurring as lenses in low-grade metaclastics (Şengün et al. 2011, 2014), yield younger ages between 65 and 69 Ma (Maastrichtian) for the eclogite facies metamorphism (Okay and Satır 2000b). However, in the Kemer metamorphic complex, which is regarded to be the

northwestern equivalent of Çamlıca metamorphics, white micas give more scattered Rb–Sr ages ranging between 84 and 65 Ma for blueschist metamorphism (Aygül et al. 2012). Similarly, timing of the blueschist facies metamorphism in southern Thrace is constrained to ca. 86 Ma by Rb–Sr and Ar–Ar phengite ages (Topuz et al. 2008). In general, the HP event documented in the Biga Peninsula is ascribed to an ongoing northward subduction of oceanic lithosphere, the Intra-Pontide Ocean, under a northern continent, i.e., the Rhodope Massif; during Albian to Maastrichtian time (Okay and Satır 2000b; Topuz et al. 2008; Aygül et al. 2012).

In the Anatolides, the metamorphic equivalents of the Taurides, Late Cretaceous HP metamorphism have been recognized in many tectonic zones (Fig. 19), from north to south, Tavşanlı Zone, Afyon Zone and Ören Unit of Lycian Nappes. Tavşanlı Zone is defined by well-preserved lawsonite-glaucophane metabasites and jadeite-bearing metaclastics (Okay 2002; Okay et al. 1998) with very rare eclogite occurrences (Whitney and Davis 2006; Çetinkaplan et al. 2008). HP metamorphism of the Tavşanlı zone was dated at ca. 80 Ma, Campanian, by white mica Rb–Sr and Ar–Ar dating techniques (Sherlock et al. 1999). Afyon
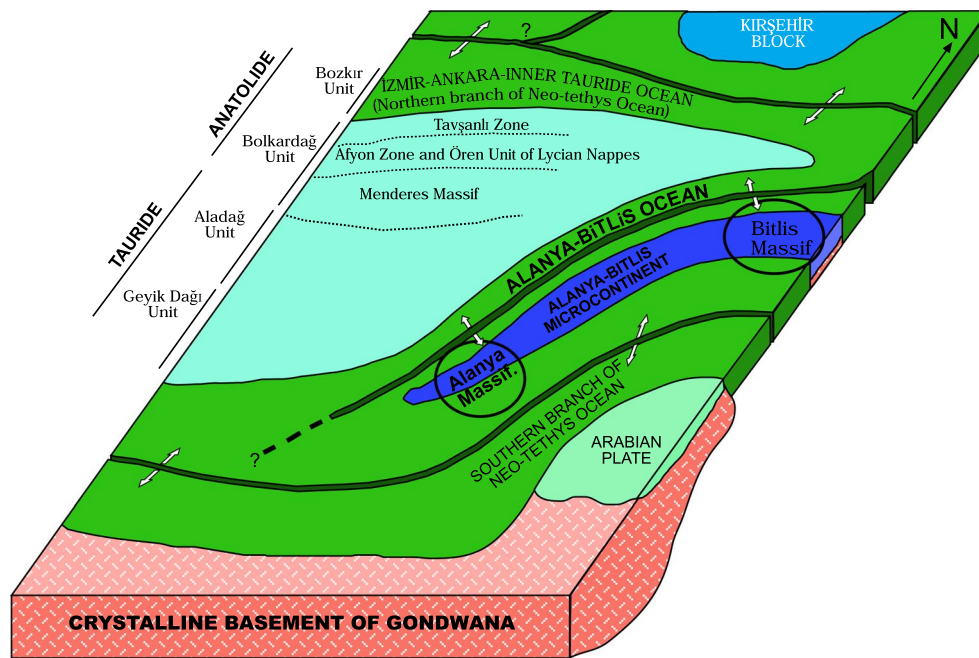
Fig. 19 Tectonic setting of Alanya and Bitlis Massifs in Albian

Zone and its southern equivalents, the Lycian Nappes (Ören unit), form an E–W-trending continuous belt, at least 600 km in length. HP/LT metamorphism is characterized by carpholite occurrences in Al-rich metasediments and rare sodic amphibole in metabasites (Candan et al. 2005; Pourteau et al. 2010, 2013; Rimmele et al. 2005, 2006). Early retrograde stages of this blueschist facies metamorphism were dated at ca. 70–65 Ma, Maastrichtian (67–62 Ma in the Afyon Zone and 63–59 Ma in the Lycian Nappes) by white mica Ar/Ar geochronology (Pourteau et al. 2013). These HP zones are interpreted to be the result of the northward subduction of the Anatolide–Tauride block under the Sakarya Zone (Pontides) in the west and under the Central Anatolian Block (Kırşehir Massif) in the east during the closure of the northern branch of the Neo-Tethys and Inner Tauride Ocean, respectively (Candan et al. 2005; Okay et al. 1998, 2001; Pourteau et al. 2010, 2013).

More recently, evidence for a Late Cretaceous HP metamorphism has been reported in the Bitlis Massif, which crops out over large areas to the south of the Anatolide–Tauride Platform in southeastern Anatolia (Oberhänsli et al. 2010, 2012, 2014). Regional distribution of carpholite, glaucophane and calcite after aragonite in the Mesozoic section of the Bitlis Massif records a HP/LT event under blueschist facies conditions. $^{39}Ar/^{40}Ar$ white mica dating gives ages of 79–74 Ma, Campanian, for the peak metamorphic assemblage of the blueschist metasediments and 69–72 Ma for their retrograde overprint under greenschist facies conditions (Fig. 12). Additionally, some eclogites in

the Precambrian basement of the Bitlis Massif yield Late Cretaceous U–Pb zircon ages of ca. 84–82 Ma for eclogite facies metamorphism, which coincides well with the slightly younger blueschist ages (Oberhänsli et al. 2014). In addition, white mica and whole rock K–Ar ages of 74–71 Ma were estimated for HP metamorphism by Göncüoglu and Turhan (1984) and Hempton (1985) in Bitlis Massif. In the tectonic model suggested for the Cretaceous HP metamorphism (Oberhänsli et al. 2012), the Bitlis Massif is assumed to be a continental block/microcontinent located between the Anatolide–Tauride Platform in the north and the Arabian Plate in the south. This continental block separates the southern Neo-Tethys into two distinct oceanic branches. The HP/LT metamorphism was caused by the consumption of the northern branch by a northward subduction and burial of the Bitlis block under the southern margin of the Anatolide–Tauride Platform during the Late Cretaceous, while the complete closure of the southern ocean, i.e., southern Neo-Tethys, and continental collision between Arabian plate and the already exhumed Bitlis Massif took place during the middle Miocene (Yılmaz 1993).

In a similar manner to that inferred for the Bitlis Massif, in a number of paleogeographical maps, the Alanya Massif is also located to the south of the Taurides as an isolated continental fragment (microcontinent and/or block), which is separated by an oceanic basin (Güzelsu Ocean; Robertson et al. 1991 or Alanya ocean; Robertson and Ustaömer 2011; Robertson et al. 2013) to the north from the Anatolide–Tauride platform (Özgül 1983; Okay and Özgül

1984; Okay 1989; Robertson 2000; Robertson et al. 1991, 2013; Garfunkel 2004; Çetinkaplan et al. 2009). This paleogeographic setting is of crucial importance and clearly precludes any possible correlations between the Alanya Massif and the Cretaceous HP belts derived from both northern branch of Neotethys and oceanic basins occurring in the Pontides. Although a similar paleogeographic position to the south of the Anatolide–Tauride Platform can be inferred for both Alanya and Bitlis blocks, the relationship between these fragments, i.e., isolated small microcontinents or a single continental sliver, spatial and temporal comparison of their Late Cretaceous subduction-related metamorphic histories and the subduction polarity of the inferred ocean have been debated for a long time (Robertson et al. 2013).

Our recent petrological and geochronological data (Fig. 19) clearly indicate a very similar tectonometamorphic evolution for both Alanya and Bitlis Massifs (Çetinkaplan et al. 2009; Oberhänsli et al. 2010, 2011, 2014). Thus, based on the *P–T–t* coherence between these two Massifs, we can suggest that both Massifs have been derived from the closure of the same ocean (*Alanya–Bitlis Ocean*) located to the south of the Anatolide–Tauride Platform. Both Alanya Massif and crystalline rocks of SE Anatolia, Bitlis, Malatya, Pütürge and Keban Massifs, occur as dismembered bodies (Yılmaz 1993; Çetinkaplan et al. 2009; Oberhänsli et al. 2010). Their original tectonic settings and lateral continuities were obscured by post-metamorphic thrusting. Although a direct correlation among these Massifs remains uncertain due to the late stage polyphase deformation, in the general tectonic classification of the Anatolides–Taurides (Özgül 1976, 1983), Alanya Massif and southeastern Anatolian crystalline rocks are inferred to be the same tectonic unit of the Taurides (Özgül 1976; Perinçek and ve Kozlu 1983; Çetinkaplan et al. 2009). Additionally, Şengör and Yılmaz (1981) suggest that Alanya and Bitlis could be a single continental sliver, which was separated from the main body of the Anatolide–Tauride Platform. Early Jurassic to Early Cretaceous times are inferred for the separation of this continental fragment (Şengör and Yılmaz 1981; Özgül 1983; Barrier and Vrielynck 2009). As emphasized in many papers (Okay and Özgül 1984; Marcoux et al. 1989; Robertson et al. 1991, 2013; Robertson 2000; Robertson and Woodcock 1984), the original tectonic situation of the Alanya Massif, which can be used to infer the subduction polarity of the Alanya–Bitlis Ocean, was destroyed by the post-metamorphic back-thrusts. As a consequence of Middle Eocene northward back-thrusting (Okay and Özgül 1984), the Alanya Massif and underlying Antalya unit were emplaced over the autochthonous Tauride platform. However, based on regional considerations and the common northward subduction polarity of the oceanic branches elsewhere in the eastern Mediterranean, a northward subduction has been inferred during the

closure of the Alanya–Bitlis Ocean (Karaoglan et al. 2012; Oberhänsli et al. 2010; Okay and Özgül 1984; Parlak et al. 2009, 2012; Robertson 2000; Robertson and Woodcock 1984; Robertson et al. 1991, 2012, 2013; Rolland et al. 2012). Consequently, we can suggest that Alanya and Bitlis Massifs could form the western and eastern parts of a single continental sliver (*Alanya–Bitlis microcontinent*), which was rifted from the southern part of the Anatolide–Tauride Platform, most probably during Early Jurassic time (Fig. 20). Furthermore, this ocean, separated from the Southern Neo-Tethys to the south by the Alanya–Bitlis microcontinent, was closed by northward subduction and deeply buried continental crust and associated accretionary complex, Sugözü and Gündoğmuş nappes, underwent HP metamorphism during the Late Cretaceous.

The relationship between Pamphylian–Alanya–Bitlis sutures

In the palinspastic restorations, the original relative arrangement of tectono-stratigraphic units of the Anatolide–Taurides, which pertained to the northern margin of Gondwana until Triassic rifting (Şengör et al. 1984; Stampli and Borel 2002; Göncüoğlu et al. 2003; Torsvik and Cocks 2013) is suggested, from north to south, as Bozkır, Bolkar Dağı, Aladağ, Geyik Dağı, Alanya and Antalya units (Özgül 1976, 1984). In many tectonic maps of Turkey, the boundary separating the autochthonous Tauride platform, Geyik Dağı unit, to the north from both the Antalya unit and Alanya Massif to the south is inferred as a suture zone, the Pamphylian suture (Fig. 18, Okay et al. 2001). The Early Paleozoic stratigraphy of the Antalya unit, which is characterized, especially, by a coherent succession of Early Cambrian quartzite, nodular limestone and Cambro–Ordovician homogenous shales has been well documented (Brunn et al. 1971; Özgül 1976; Marcoux 1979; Dean et al. 1999). The existence of the same early Paleozoic rock succession in the Alanya Massif, which was masked by polyphase metamorphism and internal imbrication, has been revealed obviously in many localities (Öztürk et al. 1995; Çetinkaplan et al. 2009). This stratigraphic correlation may allow us to suggest that the Alanya and Antalya units can be interpreted as a single unit, and that the Alanya Massif is the metamorphic equivalent of the Antalya unit. Thus, we can propose that following the Triassic rifting of the Anatolide–Tauride platform from Gondwana, the Alanya–Bitlis Ocean might have opened on the southern part of this isolated Anatolide–Tauride block corresponding to the Alanya–Antalya unit. In our tectonic model given below, the closure of the Alanya–Bitlis Ocean by northward subduction under the autochthonous Tauride platform, Geyik Dağ unit, is suggested. In this case, the suture zone representing the boundary between the upper

Fig. 20 Schematic geodynamic cross-sections showing the subsequent stages of subduction and exhumation history of the Alanya Massif. *SSZ* supra subduction zone
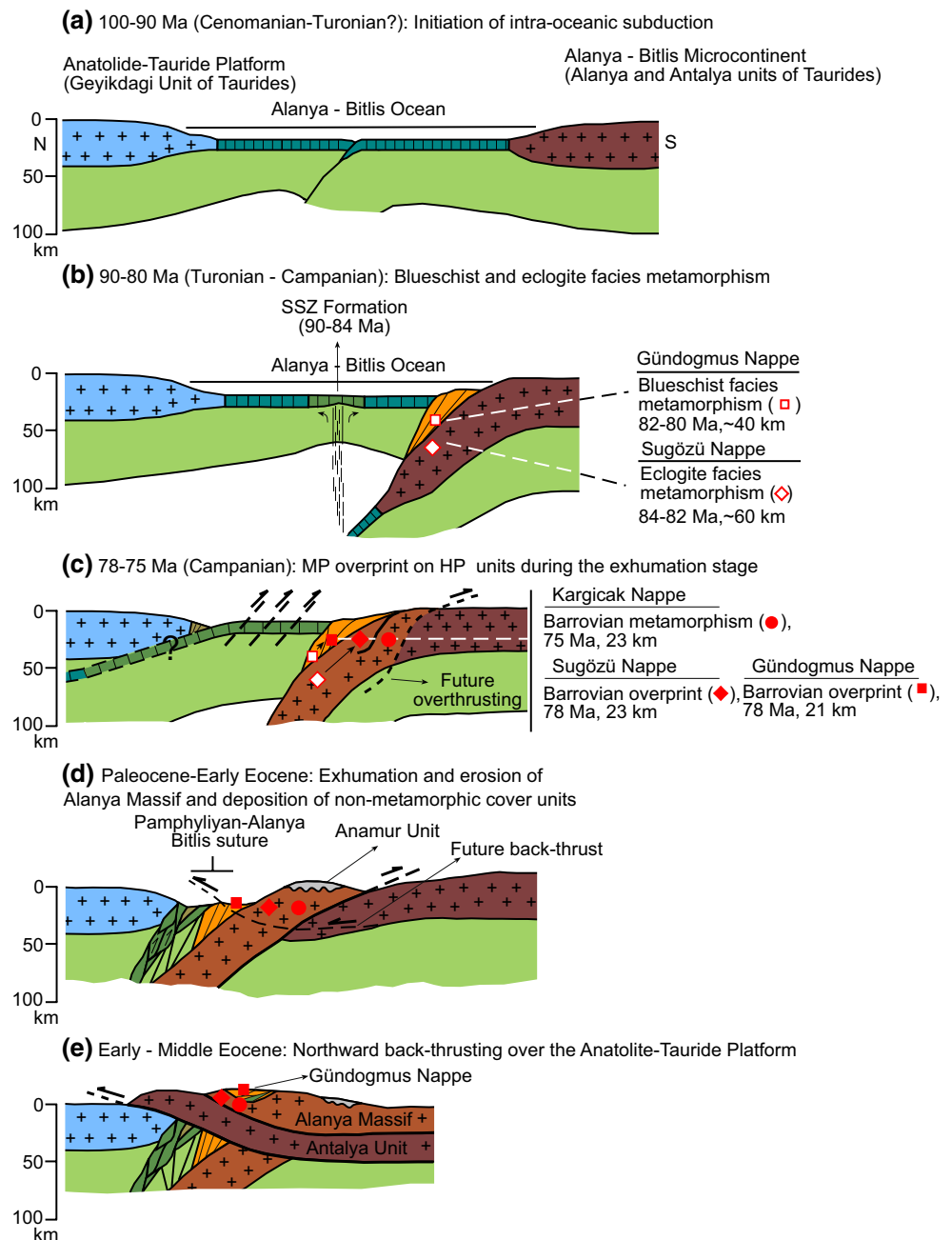
plate, autochthonous Tauride platform and the lower plate consisting of the Antalya unit and its buried equivalent, the Alanya Massif, is consistent with the inferred Pamphylian suture zone.

As discussed above, based on their paleogeographical positions and very similar *P–T–t* evolutions, we envisage that both the Alanya and Bitlis Massifs might have formed by the closure of the same oceanic branch. Although the original relations have been mostly obscured by late stage deformation and are covered by widespread young volcanic and sedimentary units, the existence of a suture zone, Muş

suture, has been postulated just to the north of Muş–Van by Şengör et al. (2008). HP evidence is only restricted to Bitlis domain (Oberhänsli et al. 2012) and any HP evidence on Keban–Kemaliye–Tunceli metamorphics forming the northern crystalline segments of the SE Anatolian crystalline rocks has not been documented yet. Considering these diverse metamorphic histories of these crystalline segments, in SE Anatolia, the inferred suture zone (Pamphylian–Alanya–Bitlis suture zone) for the Bitlis Massif should be placed to somewhere between the south of the Keban–Kemaliye–Tunceli metamorphics and north of

Bitlis metamorphics (Fig. 18). In recent studies, the existence of Late Cretaceous low-grade metamorphic rocks in northern Cyprus, the Kyrenia Range, have been reported (Robertson et al. 2011, 2012, 2013). In their tectonic models, Kyrenia is assumed to be a microcontinent separated by an oceanic basin, the Alanya Ocean, to the north from the Anatolide–Tauride platform. This paleogeographic setting is consistent with that of the Alanya–Bitlis block. No evidence indicating HP metamorphism has been found in the Kyrenia area. However, considering the existence of limited HP evidence in the Alanya Massif, which is recorded only in two thrust sheets, this cannot be used as the only discriminate feature for the correlation. Thus, based on regional considerations and the coincidence of the ages of metamorphism, we can suggest that the metamorphic rocks in Kyrenia can be correlated with the Alanya and Bitlis Massifs and, as a consequence, the suture zone connecting Alanya to Bitlis should be placed somewhere in the Cilicia Basin within continental basement (Calon et al. 2005) occurring between Cyprus and Turkey (Fig. 18).

Considering our petrological and geochronological data for the Alanya Massif, we propose a geodynamic scenario including subsequent stages from Late Cretaceous subduction of the Alanya–Bitlis Ocean to Eocene back-thrusting of the already assembled Alanya and Antalya units over the autochthonous Tauride platform (Fig. 20). There is no direct evidence indicating the onset of the subduction for the Alanya–Bitlis Ocean. For the Gündoğmuş nappe, which represents a blueschist accretionary complex, a Late Cretaceous age (Robertson et al. 2013) is assigned. Similar Late Cretaceous age for Alakır Çay mélange in Kemer, which can be postulated as the unmetamorphosed equivalent of the Gündoğmuş nappe, is suggested. Additionally, it has been revealed by Karaoğlan et al. (2012) that based on the geochemical characters, the ophiolites generated from the ocean (Berit ocean) corresponding to the eastern part of Alanya–Bitlis ocean formed as SSZ-type ophiolites and the crystallization age of these oceanic crust materials is at around 84–90 Ma (Turonian–Santonian). Considering these geological restrictions, a pre-Late Turonian age (>90 Ma), probably Cenamonian–Turonian, can be envisaged for the onset of subduction of the Alanya–Bitlis Ocean (Fig. 20a). P–T estimations (435–480 °C/11–13 kbar) and the geochronological data (80–82 Ma) indicate that part of the tectonic slice of the accretionary complex corresponding to the Gündoğmuş unit was subducted to a depth of about ~40 km and underwent blueschist metamorphism during Campanian time. Furthermore, the P–T conditions (550–567 °C/14–18 kbar) and phengite (84 Ma), zircon (84 Ma) and rutile ages (82 Ma) of the Sugözü nappe, which represent the continental material, reveal that during Santonian–Campanian time, the Alanya–Bitlis microcontinent was also buried under oceanic crust of Alanya–Bitlis Ocean and

suffered eclogite facies metamorphism at a depth of ~60 km (Fig. 20b). During this stage, as a consequence of ongoing intra-oceanic subduction, SSZ-type ophiolites (90–84 Ma, Karaoğlan et al. 2012) were generated in Alanya–Bitlis Ocean (Fig. 20b). The tectonic units in the Alanya Massif, except for Sugözü and Gündoğmuş nappes, underwent single-stage Barrovian-type (525–555 °C/6.5–7.5 kbar) metamorphism under greenschist/lower amphibolite facies conditions at about 75 Ma, Campanian. The age of this Barrovian-type medium-grade metamorphism coincides well with the greenschist–amphibolite overprint of the HP units (Sugözü and Gündoğmuş: 78 Ma, Campanian). This petrological evidence and age data indicate that during Campanian time, deeply buried units of the Alanya Massif started to uplift and were juxtaposed tectonically with the medium-grade units of the Alanya Massif at a depth of 21–23 km (Fig. 20c). Considering the absence of a large-scale ophiolite obduction over Alanya–Bitlis microcontinent, similar to the double-subduction models suggested for the Bitlis part of this ocean (Parlak 2006; Parlak et al. 2004; Robertson et al. 2006), a new low-angle subduction beneath the Anatolide–Tauride platform can be speculated for the consumption of the ocean (Fig. 20c). Based on the youngest unmetamorphosed cover unit (Paleocene–Early Eocene) on the Alanya Massif, a Paleocene age for the exhumation of the Alanya Massif and southward overthrusting onto the Antalya part of the microcontinent can be inferred (Fig. 20d). Furthermore, considering the tectonic contact between the Antalya unit and underlying Lower Eocene carbonates of the autochthonous Tauride platform and transgressive contact relationship of Lutetian conglomerates (Anamur unit) over the Alanya nappes (Okay and Özgül 1984), the northward back-thrusting of the assembled Alanya and Antalya units over the autochthonous Tauride platform can be constrained between Early and Middle Eocene (Fig. 20e). The original suture zone between Anatolide–Tauride Platform and Alanya–Antalya units was obscured by this late stage young tectonic event (Fig. 20e).

Conclusions

The Alanya Massif is made up of a number of nappe units with distinct metamorphic history. In two thrust sheets, Sugözü and Gündoğmuş nappes, HP metamorphism under eclogite (550–567 °C/14–18 kbar) and blueschist facies (435–480 °C/11–13 kbar) conditions have been recognized, while the rest of the Massif has experienced Barrovian-type medium-pressure metamorphism under greenschist–amphibolite facies (525–555 °C/6.5–7.5 kbar) conditions. Based on the stratigraphic similarities and their relative paleogeographic position, the Alanya Massif can be regarded as the metamorphic equivalent of the Antalya unit. Alanya

and Antalya units were rifted, most probably during Jurassic time, from the southern part of the Anatolide–Tauride platform and formed an isolated microcontinent/continental sliver (*Alanya–Bitlis microcontinent*), which was separated to the north from Anatolide–Tauride platform by an ocean, the *Alanya–Bitlis Ocean*, and to the south from Gondwana by the southern branch of Neo-Tethys. The closure of the Alanya–Bitlis Ocean by intra-oceanic northward subduction resulted in HP metamorphism of the deeply buried northern end of the microcontinent and accretionary complex during the Santonian–Campanian (84–80 Ma). The petrological and geochronological evidence indicate that during the exhumation stage, HP units were tectonically juxtaposed with the other Barrovian-type medium-grade tectonic units of the Alanya Massif at a depth of 21–23 km and were retrogressed under greenschist–amphibolite facies conditions during Campanian time (75–78 Ma). Based on the Late Paleocene–Eocene sedimentary cover of the Alanya Massif, the exhumation of the Alanya Massif can be constrained between Campanian and Paleocene. Considering their paleogeographic positions and similar Late Cretaceous *P–T–t* evolutions, we can suggest that both Alanya and Bitlis Massifs were derived from the western and eastern parts of the same microcontinent, the Alanya–Bitlis microcontinent, by the closure of the Alanya–Bitlis Ocean located to the south of the Anatolide–Tauride platform. The suture zone (*the Pamphylian–Alanya–Bitlis suture*) connecting Alanya to Bitlis should be placed somewhere in the Cilicia Basin within continental basement occurring between Cyprus and Turkey.

References

Ai Y (1994) A revision of the garnet–clinopyroxene Fe^{2+}–Mg exchange geothermometer. Contrib Mineral Petrol 115:467–473

Andersen T (2002) Correction of common lead in U–Pb analyses that do not report 204Pb. Chem Geol 192:59–79

Aygül M, Topuz G, Okay AI, Satir M, Meyer HP (2012) The kemer metamorphic complex (NW Turkey): a subducted continental margin of the Sakarya zone. Turk J Earth Sci 21:19–35

Barrier E, Vrielynck B (eds) (2009) Palaeotectonic maps of the Middle East. Middle East Basins Evol Program, Paris

Berman RG (1988) Internally-consistent thermodynamic data for minerals in the system Na_2O–K_2O–Ca–MgO–FeO–Fe_2O_3–Al_2O_3–SiO_2–TiO_2–H_2O–CO_2. J Petrol 29(2):445–522

Brunn JH, Dumont JH, de Graciansky PCh, Gutnic M, Juteau Th, Marcoux J, Monod O, Poisson A (1971) Outline of the geology of the western Taurids Geology and History of Turkey de: Petroleum exploration Society of Libya, Tripoli, pp 225–255

Calon TJ, Aksu AE, Hall J (2005) The Oligocene-Recent evolution of the Mesaoria Basin(Cyprus) and its western marine extension, Eastern Mediterranean. Mar Geol 221:95–120

Candan O, Dora OÖ, Oberhänsli R, Oelsner F, Dürr S (1997) Blueschist relicts in the Mesozoic cover series of the Menderes Massif and correlations with Samos Island. Cyclades Schweiz Mineral Petrogr Mitt 77:95–99

Candan O, Dora OÖ, Oberhänsli R, Çetinkaplan M, Partzsch JH, Warkus F, Dürr S (2001) Pan-African high-pressure metamorphism in the Precambrian basement of the Menderes Massif, Western Anatolia, Turkey. Int J Earth Sci (Geologische Rundschau) 89(4):793–811

Candan O, Çetinkaplan M, Oberhänslı R, Rimmelé G, Akal C (2005) Fe–Mg carpholite as a record of Alpine high-P/low-T metamorphism of Afyon Zone and implication for metamorphic evolution of western Anatolia, Turkey. Lithos 84:102–124

Çetinkaplan M, Candan O, Oberhänsli R, Romain B (2008) Pressure–temperature evolution of lawsonite eclogite in Sivrihisar; Tavşanlı Zone-Turkey. Lithos 104:12–32

Çetinkaplan M, Candan O, Okay AI, Oberhänsli R, Koralay OE, Kozlu H (2009) Tectonostratigraphy and polimetamorphic evolution of the Alanya Massif. 62nd Geological Kurultai of Turkey, 13–17 April 2009, MTA–Ankara, Türkiye. Abstract Book, pp 26–27

Çetinkaplan M, Oberhänsli R, Candan O, Koralay E, Okay AI, Kozlu H (2011) P–T–t evolution of the metamarphic rocks of Alanya Massif, 64th Geological congress of Türkiye, abstract book, pp 223–224

Cherniak DJ (2000) Pb diffusion in rutile. Contrib Mineral Petrol 139:198–207

Corfu F, Easton RM (1995) U–Pb geochronology of the Mazinaw terrane, an imbricate segment of the Central metase-dimentary belt, Grenville province, Ontario. Can J Earth Sci 32:959–976

de Capitani C, Brown TH (1987) The computation of chemical equilibrium in complex systems containing non-ideal solutions. Geochim Cosmochim Acta 51:2639–2652

de Capitani C, Petrakakis K (2010) The computation of equilibrium assemblage diagrams with Theriak/Domino software. Am Mineral 95:1006–1016

Dean WT, Uyeno TT, Rıckards RB (1999) Ordovician and Silurian stratigraphy and trilobites, Taurus Mountains near Kemer, southwestern Turkey. Geol Mag 136(4):373–393

Demirtaşlı E (1983) Stratigraphy and tectonics of the area between Silifke and Anamur, Central Taurus Mountains. In: Tekeli O, Göncüoğlu MC (eds) International symposium on the geology of the Taurus Belt, Ankara-Turkey, pp 101–118

Di Vincenzo G, Viti C, Rocchi R (2003) The effect of chlorite interlayering on 40Ar–39Ar biotite dating: an 40Ar–39Ar laserprobe and TEM investigation of variably chloritised biotites. Contrib Mineral Petrol 145:643–658

Ellis DJ, Green DH (1979) An experimental study of the effect of Ca upon garnet–clinopyroxene Fe–Mg exchange equilibria. Contrib Mineral Petrol 71:13–22

Ferry JM, Watson EB (2007) Newthermodynamicmodels and revised calibrations for the Ti-in-zircon and Zr-in-rutile thermometers. Contrib Mineral Petrol 154:429–437

Gao XY, Zheng YF, Xia XP, Chen YX (2014) U–Pb ages and trace elements of metamorphic rutile from ultrahigh-pressure quartzite in the Sulu orogen. Geochim Cosmochim Acta. doi:10.1016/j.gca.2014.04.032

Garfunkel Z (2004) Origin of the Eastern Mediterranean basin: a re-evalaution. Tectonophysics 391:11–34

Göncüoğlu MC, Turhan N (1984) Geology of the Bitlis metamorphic belt. In: TekeliO, Göncüoğlu MC (eds) Proceedings of the ınternational symposium on the geology of the Taurus Belt, pp 237–244

Göncüoğlu MC, Turhan N, Tekin UK (2003) Evidence for the Triassic rifting and opening of the Neotethyan Izmir-Ankara Ocean, northern edge of the Tauride-Anatolide Platform, Turkey. Boll Soc Geol Ital Spec 2:203–212

Graham CM, Powell R (1984) A garnet-hornblende geothermometer: calibration testing and application to the Pelona schist, Southern California. J Metamorph Geol 2:13–31

Green DH, Hellman PL (1982) Fe–Mg partitioning between coexisting garnet and phengite at high pressure, and comments on a garnet–phengite geothermometer. Lithos 15:253–266

Hempton MR (1985) Structure and deformation history of the Bitlis Suture near Lake Hazar, SE Turkey. Geol Soc Am Bull 96:223–243

Hodges KV, Spear FS (1982) Geothermometry, geobarometry and the Al2SiO5 triple point at Mt. Moosilauke, new Hampshire. Am Mineral 67(1118–1134):25

Hoisch TD (1991) Equilibria within the mineral assemblage quartz + muscovite + biotite + garnet + plagioclase, and implications for the mixing properties of octahedrally-coordinated cations in muscovite and biotite. Contrib Mineral Petrol 108:43–54

Holland TJB, Powell R (1998) An internally-consistent thermodynamic dataset for phases of petrological interest. J Metamorph Geol 16:309–344

Işık V, Tekeli O (1995) Alanya metemorfiklerinin doğu kesiminde yer alan petrografik bulgular. MTA dergisi 117:105–113

Jowett EC (1991) Fitting iron and magnesium into the hydrothermal chlorite geothermometer: GAC/MAC/SEG joint annual meeting (Toronto, May 27–29, 1991). Program Abstr 16:A62

Karaoğlan F, Parlak O, Klotzi U, Thoni M, Koller F (2012) U–Pb and Sm–Nd geochronology of the ophiolites from the SE Turkey: implications for the Neotethyan evolution. Geodin Acta 25(3–4):146–161

Ketin İ (1966) Anadolu'nun tektonik birlikleri. MTA Derg 66:20–34 (Ankara)

Kooijman E, Mezger K, Berndt J (2010) Constraints on the U–Pb systematics of metamorphic rutile from in situ LA-ICP-MS analysis. Earth Planet Sci Lett 293:321–330

Koziol AM, Newton RC (1988) Re-determination of the anorthite breakdown reaction and improvement of the plagioclase–garnet–Al$_2$SiO$_5$–quartz barometer. Am Mineral 73:216–223

Krogh EJ (1988) The garnet–clinopyroxene Fe–Mg geothermometer a re-interpretation of existing experimental data. Contrib Mineral Petrol 99:44–48

Krogh EJ, Raheim A (1978) Temperature and pressure dependence of Fe–Mg partitioning between garnet ahd phengite with particular reference to eclogites. Contrib Mineral Petrol 66:75–80

Krogh Ravna E (2000) The garnet–clinopyroxene Fe24–Mg geothermometer: an updated calibration. J Metamorph Geol 18:211–219

Leake BA, Woolley AR, Arps CES, Birch WD, Gilbert MC, Grice JD, Hawthorne FC, Kato A, Kisch HJ, Krivovichev VG, Linthout K, Laird J, Mandarino J, Maresch WV, Nickel EH, Rock NMS, Schumacher JC, Smith DC, Stephonson NCN, Ungaretti L, Whittaker EJW, Youzmi G (1997) Nomenclature of amphiboles. Report of the Subcommittee on Amphiboles of the International Mineralogical Association Commission on New Minerals and Mineral Names. Eur J Mineral 9:623–651

Li QL, Li SG, Zheng Y-F, Li H, Massonne HJ, Wang Q (2003) A high precision U–Pb age of metamorphic rutile in coesite-bearing eclogite from the Dabie mountains in central China: a new constraint on the cooling history. Chem Geol 200:255–265

Li QL, Lin W, Sun W, Li XH, Shi YH, Liu Y, Tang GQ (2011) SIMS U–Pb rutile age of low-temperature eclogites from southwestern Chinese Tianshan, NW China. Lithos 122:76–86

Ludwig KR (2012) User's manual for Isoplot 3.75: a geochronological toolkit for microsoft excel. Berkeley Geochronology Center Special Publication No 5, USA

Luvizotto GL, Zack T (2009) Nb and Zr behavior in rutile during high-grade metamorphism and retrogression: an example from the Ivrea-Verbano Zone. Chem Geol 261:303–317

Marcoux J (1979) General features of Antalya nappes and their significance in the paleogeography of southern margin of Tethys. Bull Geol Soc Turk 22:1–5

Marcoux J, Ricou LE, Burg X, Brunn JP (1989) Shear sense criteria in the Antalya and Alanya thrust system (southwestern Turkey): evidence for a southward emplacement. Tectonophysics 161:81–91

Massonne H-J, Szpurka Z (1997) Thermodynamic properties of white micas on the basis of high-pressure experiments in the systems K$_2$O–MgO–Al$_2$O$_3$–SiO$_2$–H$_2$O and K$_2$O–FeO–Al$_2$O3–SiO$_2$–H$_2$O. Lithos 41:229–250

McDougall I, Harrison TM (1999) Geochronology and thermochronology by the 40Ar/39Ar method. Oxford University Press, New York

Mezger K, Rawnsley C, Bohlen SR, Hanson GN (1991) U-Pb garnet, sphene, monazite, and rutile ages: implications for the duration of high-grade metamorphism and cooling histories Adirondack Mountains, New York. J Geol 99:415–428

Monod O, Kuzucuoğlu C, Okay AI (2006) A Miocene paleovalley network in the Western Taurus (Turkey). Turk J Earth Sci 15:1–23

Morimoto N, Fabries J, Ferguson AK, Ginzburg IV, Ross M, Seifert FA, Zussman JZ (1988) Nomenclature of pyroxenes. Am Mineral 73:1123–1133

Nakamura D (2009) A new formulation of garnet–clinopyroxene geothermometer based on accumulation and statistical analysis of a large experimental data set. J Metamorph Geol 27(7):495–508

Oberhänsli R, Monie P, Candan O, Warkus F, Partzsch JH, Dora OÖ (1998) The age of blueschist metamorphism in The Mesozoic cover series of the Menderes Massif. Schweiz Mineral Petrogr Mitt 78:309–316

Oberhänsli R, Candan O, Bousquet R, Rimmele G, Okay A, Goff J (2010) Alpine HP evolution of the eastern Bitlis complex, SE Turkey. In: Sosson M, Kaymakci N, Stephenson R, Strarostenko V, Bergerat F (eds) Sedimentary basins, tectonics from Black Sea an Caucasus to the Arabian platform. Geol Soc Lond Spec Publ 340:461–483

Oberhänsli R, Pourteau A, Candan O, Çetinkaplan M, Bousquet R (2011) High pressure in the Anatolide–Tauride belt. In: 9th international eclogite conference 2011, Abstract volume (2), p 54

Oberhänsli R, Bousqueti R, Candan O, Okay A (2012) Dating Subduction Events in East Anatolia, Turkey. Turk J Earth Sci 12:1–17

Oberhänsli R, Koralay E, Candan O, Pourteau A, Bousquet R (2014) Late Cretaceous eclogitic high-pressure relics in the Bitlis Massif. Geodin Acta. doi:10.1080/09853111.2013.858951

Okay AI (1986) High pressure/low temperature metamorphic rocks of Turkey. In: Evans BW, Brown EH (ed) Blueschists and eclogites. Geol Soc Am Memoir 164:333–348

Okay AI (1989) An exotic eclogite/blueschist slice in a Barrovian-style metamorphic terrain, Alanya Nappes, Southern Turkey. J Petrol 30 Part 1:107–132

Okay AI (2002) Jadeite–chloritoid–glaucophane–lawsonite schists from northwest Turkey: unusually high P/T ratios in continental crust. J Metamorph Geol 20:757–768

Okay AI, Monié P (1997) Early Mesozoic subduction in the Eastern Mediterranean: evidence from Triassic eclogite in northwest Turkey. Geology 25:595–598

Okay AI, Özgül N (1984) HP/LT metamorphism and structure of the Alanya Massif, Southern Turkey: an allochthonous composite tectonic sheet. In: Robertson AHF, Dixon TE (ed) The geological evolution of the Eastern Mediterranean. Geol Soc Lond Spec Publ 14:429–439

Okay AI, Satır M (2000a) Coeval plutonism and metamorphism in a latest Oligocene metamorphic core complex in northwest Turkey. Geol Mag 137:495–516

Okay AI, Satır M (2000b) Upper Cretaceous eclogite facies metamorphic rocks from the Biga Peninsula, northwest Turkey. Turk J Earth Sci 9:47–56

Okay AI, Tüysüz O (1999) Tethyan sutures of northern Turkey. In: Durand B, Jolivet L, Horváth F, Séranne M (eds) The Mediterranean Basins: Tertiary extension within the Alpine orogen. Geol Soc Lond Spec Publ 156:475–515

Okay AI, Satır M, Maluski H, Siyako M, Monie P, Metzger R, Akyüz S (1996) Paleo- and Neo-Tethyan events in northwest Turkey: geological and geochronological constraints. In: Yin A, Harrison M (eds) Tectonics of Asia. Cambridge University Press, Cambridge, pp 420–441

Okay AI, Harris NBW, Kelley SP (1998) Exhumation of blueschists along a Tethyan suture in northwest Turkey. Tectonophysics 285:275–299

Okay AI, Tansel İ, Tüysüz O (2001) Obduction, subduction and collision as reflected in the Upper Cretaceous–Lower Eocene sedimentary record of western Turkey. Geol Mag 138:117–142

Okay AI, Monod O, Monié P (2002) Triassic blueschists and eclogites from northwest Turkey: vestiges of the Paleo-Tethyan subduction. Lithos 64:155–178

Okay AI, Satır M, Siebel W (2006) Pre-alpide orogenic events in the Eastern Mediterranean region. European lithosphere dynamics. Geol Soc Lond Memoirs 32:389–405

Okay AI, Sunal G, Sherlock S, Altıner D, Tüysüz O, Kylander-Clark ARC, Aygül M (2013) Early Cretaceous sedimentation and orogeny on the active margin of Eurasia: Southern Central Pontides, Turkey. Tectonics 32:1247–1271

Özgül N (1976) Toroslar'ın bazı temel jeoloji özellikleri. Türkiye Jeol Kur Bült 19:65–78

Özgül N (1983) Stratigraphy and tectonic evolution of the Central Taurides. In: Tekeli O, Göncüoğlu MC (ed) International symposium on the geology of the Taurus Belt, Ankara-Turkey, pp 77–90

Özgül N (1984) Geology of the Central Taurides. In: Tekeli O, Ve Göncüoğlu MC (ed) Proceedings of the International Symosium on geology of the Taurus Belt da. 26–29 Eylül, Ankara, pp 143–158

Öztürk EM, Akdeniz N, Bedi Y, Sönmez İ, Usta D, Kuru K, Erbay G (1995) Alanya Napının stratigrafisine farklı bir yaklaşım. TJK Bült 10:2–10

Parlak O (2006) Geodynamic significance of granitoid magmatism in the Southeast Anatolian Orogen: geochemical and geochronological evidence from Göksun-Afşin (Kahramanmaraş, Turkey) region. Int J Earth Sci 95:609–627

Parlak O, Höck V, Kozlu H, Delaloye M (2004) Oceanic crust generation in an island arc tectonic setting, SE Anatolian Orogenic Belt (Turkey). Geol Mag 141:583–603

Parlak O, Rizaoğlu T, Bağci U, Karaoğlan F, Höck V (2009) Geochemistry of Ophiolites in the Southeast Anatolia, Turkey. Tectonophysics 473:173–187

Parlak O, Karaoğlan F, Thöni M, Robertson AHF, Okay AI, Koller F (2012) Geochemistry, geochronolgy and tectonic significance of high temperature meta-ophiolitic rocks: possible relation to Eocene south-Neotethyan arc magmatism (Malatya area, SE Anatolia). 65. Geological Congress of Turkey, 2–7 April 2012, Ankara, Abstract 88–91

Perchuck LL, Lavrenteva IV (1983) Experimental investigation of exchange equilibria in the system cordierite–garnet–biotite. In: Saxena SK (ed) Kinetics and equilibrium in mineral reaction. Springer, New York

Perinçek D, ve Kozlu H (1983) Stratigraphy and structural relations of the units in the Afşin-Elbistan-Doğanşar region (Eastern Taurus). In: Tekeli O, Göncüoğlu MC (eds) Geology of the Taurus Belt. Ankara-Turkey, pp 181–197

Pourteau O, Candan, Oberhänsli R (2010) High-pressure metasediments in central Turkey: constraints on the Neotethyan closure history. Tectonics 29. doi:10.1029/2009TC002650

Pourteau A, Sudo O, Candan O, Lanari P, Vidal O, Oberhänsli R (2012) Neotethys closure history of Anatolia: insights from ^{40}Ar–^{39}Ar geochronogic data and multi-equilibrium al Research Abstracts, 14, EGU2012-4882

Pourteau A, Sudo O, Candan O, Lanari P, Vidal O, Oberhänsli R (2013) Neotethys closure history of Anatolia: insights from 40Ar–39Ar geochronology and P–T estimation in high-pressure metasedimentary rocks. J Metamorph Geol. doi:10.1111/jmg.12034

Powell R (1985) Regression diagnostics and robust regression in geothermometer/geobarometer calibration: the garnet–clinopyroxene geothermometer revisited. J Metamorph Geol 3:231–243

Rimmele G, Parra T, Goffe B, Oberhänsli R, Jolivet L, Candan O (2005) Exhumation paths of high-pressure–low-temperature metamorphic rocks from the Lycian Nappes and the Menderes Massif (SW Turkey): a multi-equilibrium approach. J. Petrology 46(3):641–669

Rimmelé G, Oberhänsli R, Candan O, Goffé B, Jolivet L (2006) The wide distribution of HP–LT rocks in the Lycian Belt (Western Turkey). Implications for the accretionary wedge geometry. J. Geol Soc Lond Spec Publ 260:447–466

Robertson AHF (2000) Mesozoic–Tertiary tectonosedimentary evolution of a south-Tethyan oceanic basin and its margins in southern Turkey. In: Bozkurt E, Winchester JA, Piper JDA (eds) Tectonics and magmatism in Turkey and surrounding area. Geol Soc Lond Spec Publ 173:97–138

Robertson A (2004) Development of concepts concerning the genesis and emplacement of Tethyan ophiolites in the Eastern Mediterranean and Oman regions. Earth Sci Rev 66:331–387

Robertson AHF, Ustaömer T (2011) Role of tectonic–sedimentary melange and Permian-Triassic cover units, central southern Turkey in Tethyan continental margin evolution. J Asian Earth Sci 40:98–120

Robertson AHF, Woodcock NH (1984) The SW segment of the Antalya complex, Turkey as a Mesozoic–Tertiary Tethyan continental margin. In: Dixon JE, Robertson AHF (eds) The geological evolution of the Eastern Mediterranean. Geol Soc Lond Spec Publ 17:251–271

Robertson AHF, Clift PD, Degnan PJ, Jones G (1991) Paleogeographic and paleotectonic evolution of the eastern Mediterranean Neotethys. Palaeogeogr Palaeoclimatol Palaeoecol 87:289–343

Robertson AHF, Ustaömer T, Parlak O, Ünlü-genç UC, Tasli K, İnan N (2006) The Berit Transect of the Tauride Thrust Belt, S. Turkey: Late Cretaceous-Early Cenozoic Accretionary/Collisional processes related to closure of the Southern Neotethys. J Asian Earth Sci 27:108–145

Robertson AHF, Taslı K, İnan N (2011) Evidence from the Kyrenia range, Cyrus, of the northerly active magrin of the southern Neotethys during late Createcous—Early Cenozoic time. Geol Mag 148:1–27

Robertson AHF, Parlak O, Ustaömer T (2012) Overview of the Palaeozoic-Neogene evolution of Neotethys in the Eastern Mediterranean region (southern Turkey, Cyprus, Syria). Pet Geosci 18:381–404. doi:10.1144/petgeo-091

Robertson AHF, Parlak O, Ustaömer T (2013) Late Paleozoic-Early Cenozoic tectonic development of southern Turkey and the easternmost Mediterranean region: evidence from the inter-relations of continental and oceanic units. Geol Soc Lond Spec Publ 3793:9–48

Rolland Y, Billo S, Corsini M, Sosson M, Galoyan G (2009) Blueschists of the Amassia-Stepanavan Suture Zone (Armenia):

linking Tethys subduction history from E-Turkey to W-Iran. Int J Earth Sci 98(3):533–550

Rolland Y, Perinçek D, Kaymakci N, Sosson M, Barrier E, Avagyane A (2012) Evidence for_80–75 Ma subduction jump during Anatolide–Tauride–Armenian block accretion and _48 Ma Arabia-Eurasia collision in Lesser Caucasus–East Anatolia. J Geodyn 56–57:76–85

Şenel M, Dalkılıç H, Gedik İ, Serdaroğlu M, Bölükbaşı AS, Metin S, Esentürk K, Özgül Z (1999) Orta Toroslar'da Güzelsu Koridoru ve kuzeyinin Jeolojisi. Türkiye Jeol Kur Bült 2(1):30–40

Şengör AMC, Yılmaz Y (1981) Tethyan evolution of Turkey: a plate tectonic approach. Tectonophysics 75:181–241

Şengör AMC, Yılmaz Y, Ketin I (1980) Remnants of a pre-Late Jurassic ocean in the northern Turkey: fragments of Permian-Triassic Paleo-Tethys? Geol Soc Am Bull 91(1):599–609

Şengör AMC, Satır M, Akkök R (1984) Timing of tectonic events in the Menderes Massif, western Turkey: implications for tectonic evolution and evidence for Pan-African basement in Turkey. Tectonics 3:693–707

Şengör AMC, Görür N, Şaroğlu F (1985) Strike-slip faulting and related basin formation in zones of tectonic escape: Turkey as a case study. In: Biddle KT, Christie-Blick N (eds), Strike-slip deformation, Basin formation and sedimentation. Soc Econ Mineral Paleontol Spec Publ 37:227–264

Şengör AMC, Özeren MS, Keskin M, Sakınç M, Özbakır AD, Kayan İ (2008) Eastern Turkish high plateau as a Turkic-type orogen: implications for post-collisional crust-forming processes in Turkic-type orogens. Earth Sci Rev 90:1–48

Şengün M, Avarlar M, Çetin F, Doğan ZO, Gök A (1978) Alanya Masifinin yapısal konumu. Jeoloji Mühendisliği 6:39–45

Şengün F, Yiğitbaş E, Tunç İO (2011) Geology and Tectonic emplacement of eclogite and blueschist, Biga peninsula, Northwest Turkey. Turk J Erath Sci 20:273–285

Şengün F, Davis PB, Tunç İO, Yiğitbaş E (2014) Petrology and geochemistry of eclogites from the Biga Peninsula, Northwest Turkey. Geodin Acta. doi:10.1080/09853111.2013.858954

Sherlock S, Kelley SP, Inger S, Haris N, Okay AI (1999) 40Ar–39Ar and Rb–Sr geochronology of high-pressure metamorphism and exhumation history of the Tavşanlı Zone, NW Turkey. Contrib Mineral Petrol 137:46–58

Stampli GM, Borel GD (2002) A plate tectonic model for the Paleozoic and Mesozoic constrained by dynamic plate boundaries and restored synthetic oceanic isochrons. Earth and Planetary Science Letters 196:17–33

Thompson AB (1976) Mineral reactions in pelitic rocks. II. Calculation of some P–T–X(Fe–Mg) phase relations. Am J Sci 276:425–454

Tomkins HS, Powell R, Ellis DJ (2007) The pressure dependence of the zirconium-in-rutile thermometer. J Metamorph Geol 25:703–713

Topuz G, Okay AI, Altherr R, Satır M, Schwarz H (2008) Late Cretaceous blueschist facies metamorphism in southern Thrace (Turkey) and its geodynamic implications. J Metamorph Geol 26:895–913

Torsvik HT, Cocks LRM (2013) Gondwana from top to base in space and time. Gondwana Res 24:999–1030

Villa IM (1998) Isotopic closure. Terra Nova 10:42–47

Watson EB, Wark DA, Thomas JB (2006) Crystallization thermometers for zircon and rutile. Contrib Mineral Petrol 151:413–433

Whitney D, Davis PB (2006) Why is lawsonite eclogite so rare? Metamorphism and preservation of lawsonite eclogite, Sivrihisar, Turkey. Geology 34(6):473–476

Wiederkehr M, Sudo M, Bousquet R, Berger A, Schmid SM (2009) Alpine orogenic evolution from subduction to collisional thermal overprint: the (40)Ar/(39)Ar age constraints from the Valaisan Ocean, central Alps. Tectonics 28:TC6009

Yılmaz Y (1993) New evidence and model on the evolution of the southeast Anatolian orogen. Bull Geol Soc Am 105:252–271

Yuan HL, Gao S, Liu XM, Li HM, Günther D, Wu FY (2004) Accurate U–Pb age and trace element determinations of zircon by laser ablation-inductively coupled plasma-mass spectrometry. Geostand Geoanal Res 28:353–370

Zack T, Moraes R, Kronz A (2004) Temperature dependence of Zr in rutile: empirical calibration of a rutile thermometer. Contrib Mineral Petrol 148:471–488

Zack T, Stockli DF, Luvizotto GL, Barth MG, Belousova E, Wolfe MR, Hinton RW (2011) In-situ U/Pb rutile dating by LA-ICP-MS: 208 Pb correction and prospects for thermochronological applications. Contrib Mineral Petrol. 162:515–530